Deep-Sea Research I 58 (2011) 209–228

Contents lists available at ScienceDirect

Deep-Sea Research I

journal homepage: www.elsevier.com/locate/dsri

Relative dispersion in the Liguro-Provençal basin: From sub-mesoscale to mesoscale

K. Schroeder [a], A.C. Haza [b], A. Griffa [a,b], T.M. Özgökmen [b,*], P.M. Poulain [c], R. Gerin [c], G. Peggion [d], M. Rixen [e]

[a] ISMAR-CNR, La Spezia, Italy
[b] RSMAS/MPO, University of Miami, Miami, FL 33149, USA
[c] OGS, Trieste, Italy
[d] University of New Orleans, USA
[e] NATO Undersea Research Center, La Spezia, Italy

ARTICLE INFO

Article history:
Received 19 August 2010
Received in revised form
12 November 2010
Accepted 15 November 2010
Available online 2 December 2010

Keywords:
Dispersion
Turbulence
Sub-mesoscale
Coastal transport

ABSTRACT

Relative dispersion in the Liguro-Provençal basin (a subregion of the Mediterranean Sea) is investigated using clusters of surface drifters deployed during two Marine Rapid Environment Assessment (MREA) experiments covering different months in 2007 and 2008, respectively. The clusters have initial radii of less than 1 km, or an order of magnitude below a typical deformation radius (approximately 10–20 km). The data set consists of 45 original pairs and more than 50 total pairs (including chance ones) in the spatial range between 1 and 200 km. Relative dispersion is estimated using the mean square separation of particle pairs and the Finite Scale Lyapunov Exponents (FSLEs). The two metrics show broadly consistent results, indicating in particular a clear exponential behaviour with an *e*-folding time scale between 0.5 and 1 days, or Lyapunov exponent λ in the range of 0.7–1 days^{-1}. The exponential phase extends for 4–7 days in time and between 1 and 10–20 km in separation space. To our knowledge, this is only the third time that an exponential regime is observed in the world ocean from drifter data. This result suggests that relative dispersion in the Liguro-Provençal basin is nonlocal, namely controlled mainly by mesoscale dynamics, and that the effects of the sub-mesoscale motions are negligible in comparison. NCOM model results are used to complement the data and to quantify errors arising from the sparse sampling in the observations.

1. Introduction

Relative dispersion is used in many practical applications such as understanding and predicting the spreading of pollutants and biological quantities in the ocean. It is commonly computed using the mean squared separation of particle pairs,

$$D^2(t) = \langle |\mathbf{x}^{(1)}(t) - \mathbf{x}^{(2)}(t)|^2 \rangle, \quad (1)$$

where the superscripts indicate the two particles in each pair and the average is over all pairs of particles in the cluster. $D^2(t)$ provides a description of the spreading of fluid particles under chaotic advection and turbulent motions, and it also reveals insight into the multi-scale dynamics in the ocean, since different processes are influential on the spreading at different temporal and spatial scales.

While we refer the reader to, e.g. Sawford (2001), Poje et al. (2010) for extensive discussions on relative dispersion, we summarize below several concepts that are important for the present study. The general theoretical framework for relative dispersion $D^2(t)$ is provided by 2D and quasi-geostrophic turbulence, that have been intensively investigated in the literature (Salmon, 1980; Kraichnan, 1967). One basic concept, based on dimensional arguments, is that under some conditions there is a relationship between the time behaviour of relative dispersion and the slope of the kinetic energy wave number k spectrum (Bennett, 1984). For steep spectra, characterized by k^{-a}, with $a \geq 3$, relative dispersion is expected to be exponential in time and nonlocal, in that it is dictated by the strain induced by energetic mesoscale turbulent coherent structures rather than by weaker and smaller local eddies. For less steep spectra, $1 < a < 3$, relative dispersion is expected to be local and to obey a power law, $D^2 \sim t^{4/(3-a)}$. For quasi-geostrophic turbulence forced at a single scale R (typically corresponding to the deformation radius, Salmon, 1980), two main spectral regimes are expected to occur. At scales smaller than R, the enstrophy cascade is expected to dominate, with a typical spectrum k^{-3} (or steeper in the presence of coherent vortices). At larger scales, in the energy cascade range, a much less steep spectrum of $k^{-5/3}$ is typical.

This general framework has some direct consequences in terms of relative dispersion. Three main regimes of $D^2(t)$ are expected to occur, depending on the size of particle separation D with respect to

* Corresponding author. Tel.: +1 305 421 4053; fax: +1 305 421 4696.
E-mail address: tozgokmen@rsmas.miami.edu (T.M. Özgökmen).

0967-0637/$ - see front matter © 2010 Elsevier Ltd. All rights reserved.
doi:10.1016/j.dsr.2010.11.004

the deformation radius R that characterizes the main mesoscale eddies.

For scales $D < R$, what we refer to as the sub-mesoscale range, a typical spectrum is k^{-3} or steeper and relative dispersion is expected to be exponential. In the mesoscale range, $D \geq R$, relative dispersion is expected to obey to Richardson law $D^2 \sim t^3$. Finally, for $D \gg R$, when particle pairs become uncorrelated, the same asymptotic diffusive regime as for single particles is expected to emerge, with relative dispersion growing linearly in time, $D^2 \sim t$.

Another important framework for the understanding of relative dispersion is provided by dynamical system theory (Ottino, 1989), that points out to the impact of long living coherent vortices on particle statistics (Ehlmaidi et al., 1993). In particular, pair separation near elliptic regions (e.g. inside of vortex structures where vorticity dominates strain) is expected to grow linearly in time, while an exponential regime is expected to prevail near hyperbolic regions (high strain regions between eddies and jets). The role of coherent structures in Lagrangian transport in the ocean has been addressed by a number of authors in the last few years (d'Ovidio et al., 2004; Wiggins, 2005), who put forth that much of the complex Lagrangian pathways can be explained on the basis of the temporal variability of persistent geometrical features, such as jets and eddies in the ocean.

Despite the relevance of both the turbulent and the dynamical system conceptual frameworks, a number of questions are still open, especially for complex geophysical flows such as the ocean. For instance, dynamical system methods require a precise specification of the Eulerian velocity field in two spatial dimensions and time, for which idealized (Coulliette and Wiggins, 2000) and realistic (Toner and Poje, 2004) ocean general circulation models have been employed. These models only resolve mesoscale features. Only few studies exist (Haza et al., 2007, 2010; Shadden et al., 2008) that involve ocean data and support the applicability of these concepts to the real ocean.

Regarding the turbulent approach, ocean spectra are still largely unknown, and the grand challenge posed by ocean flows is the wide range of interacting scales. In particular, existence of sub-mesoscale processes in the upper ocean have been put forward (Klein et al., 2008; Capet et al., 2008), but the interaction of sub-mesoscale and mesoscale motions has not been understood. As such, it is not clear which scales in the turbulent spectrum control the transport; is there a dominant mechanism for transport, or transport depends entirely on the local turbulent process? This is an important question because if all scales of motion play a significant role in transport, then all scales have to be observed well enough to understand and model, which is clearly a difficult task for the foreseeable future. If, on the other hand, the mesoscale features that are long-lived and contain most of the energy in the oceanic flows dictate the transport, while the imbedded sub-mesoscale motions are weak, small and transient enough perturbations are not to affect the pathways significantly, then present eddy-resolving ocean models and data assimilation methods relying on satellite altimeters with current spatial resolution capabilities would be largely satisfactory as prediction systems of ocean transport. Investigation of relative dispersion in the real multiscale environment of ocean flows provides one of the avenues to investigate this fundamental problem, and drifters from clustered arrays appear to be valuable data sets to compute relative dispersion in various locations in the ocean.

Most of the studies on relative dispersion in the ocean have been limited until recently to the mesoscale and asymptotic diffusive regimes, since sub-mesoscale studies were severely limited by model resolution and availability of particle pairs. While the world ocean has been extensively sampled by drifters over the past few decades (Lumpkin and Pazos, 2007), the main objective until recently has been to estimate the mean flow and single particle diffusivity. As such, the sampling was targeted toward single drifter launches, so that relative dispersion was typically computed using chance pairs, i.e. drifters that were not released together but that got close one to another at some time, as they were advected by the currents (LaCasce and Bower, 2000). Results from these historical works at the ocean surface (Davis, 1985; Lacorata et al., 2001) and sub-surface (LaCasce and Bower, 2000) clearly show the existence of the diffusive regime at asymptotic distances, while the mesoscale range appears to be typically characterized by Richardson regime, or by a ballistic ($D^2 \sim t^2$) regime associated with shear dispersion.

Relative dispersion in the sub-mesoscale range remains elusive, even though it has recently received growing attention using models and drifter data. The resolution of ocean general circulation models (OGCMs) has increased in the last decade, but accurate sub-mesoscale parameterizations still require dedicated efforts. There are additional factors that become important at such spatial scales, such as non-hydrostatic dynamics and vortex force arising from the interactions of waves, winds and currents, that are typically missing in most OGCMs but may play an important role in the ocean dynamics. Perhaps, the most systematic investigation of the sub-mesoscale relative dispersion in OGCMs was undertaken by Poje et al. (2010). Using a hierarchy of models from 2D turbulence to a realistic HYCOM model of the Atlantic, Poje et al. (2010) show that in all cases the initial phase of relative dispersion is characterized by an exponential regime, and the temporal extent of exponential scaling is related to the degree of spatial smoothing of the velocity field.

Regarding drifter data, a number of recent experiments have considered appropriate sampling strategy for relative dispersion, i.e. drifters launched in pairs or triplets. To our knowledge, though, only three experiments so far have allowed a quantitative computation of the sub-mesoscale phase of dispersion. LaCasce and Ohlmann (2003) consider original and chance pairs from the large SCULP data set in the Gulf of Mexico and find, for initial distances of the order of 1 km, a clear initial exponential regime with an e-folding time of 2–3 days, extending up to a separation scale of 40–50 km roughly corresponding to the deformation radius R. Koszalka et al. (2009) in the Nordic Seas (characterized by a deformation radius of less than 10 km) consider the POLEWARD set of drifters launched in pairs and triplets and, for initial distances of 2 km, find an approximately exponential behaviour for the first two days with an e-folding time of roughly 1/2 day. Lumpkin and Elipot (2010), on the other hand, find significantly different results considering drifter pairs launched in the Gulf Stream region at scales much smaller than R. In this case, the initial phase appears closer to Richardson $D^2 \sim t^3$ than to exponential law. This result is qualitatively similar to what was obtained in the atmosphere by re-examining the EOLE data (Lacorata et al., 2004), and it is reminiscent of earlier oceanographical results based on dye spreading suggesting an energy cascade at the surface (e.g. Okubo, 1971). In summary, the results on sub-mesoscale dispersion are still controversial. They are still limited to very few regions over the world ocean and show different results in terms of parameter values and observed regimes. This precludes any generalized guideline for the parametrization of sub-mesoscale spreading, and motivates further targeted studies of relative dispersion in other oceanic regions.

In this paper an investigation on relative dispersion is presented using results from a set of drifter clusters released in the Liguro-Provençal basin, a subregion of the Mediterranean Sea. Clusters of 3–5 drifters have been repeatedly released during two Marine Rapid Environmental Assessment (MREA) experiments in 2007 and 2008, respectively. Most of the clusters are launched at the same location, approximately in the center of the basin, close to the oceanographic buoy ODAS (http://www.odas.ge.issia.cnr.it/) and within the main cyclonic circulation. The region is characterized by

baroclinic variability with deformation radius R varying from less than 10 km (Marullo et al., 1985; Barth et al., 2005) to approximately 20 km (Vignudelli et al., 2003) in the long living and topographically linked structures of the main cyclonic current. A description of the data set and of the associated general circulation is given in Poulain et al. (submitted for publication).

Here, we focus on the properties of the initial, sub-mesoscale phase of relative dispersion. The data set includes a total of 45 original pairs with initial distances of less than 1 km, i.e. more than one order of magnitude smaller than R. The relative dispersion analysis is performed using two independent methods: classical pair separation statistics and Finite Scale Lyapunov Exponents (FSLEs). The drifter data results are complemented by an analysis of high resolution NCOM model results, aimed at verifying the effects of resolution and investigating sampling issues.

The paper is organized as follows. After a brief description of the drifter data and the numerical model (Section 2), a general description of the observations is proposed (Section 3.1). Particle pair statistics of drifter clusters in 2007 and 2008 are then analyzed, using relative dispersion (Section 3.2) as well as FSLEs (Section 3.3). These quantities are compared with the modeled values from NCOM outputs in Section 4. We conclude in Section 5 with a summary and a discussion on future perspectives and applications.

2. Region of interest and data sets

2.1. The Liguro-Provençal basin

The Liguro-Provençal basin is located in the northwestern Mediterranean Sea off the coasts of Italy and France (Fig. 1). It is connected to the south-east with the Tyrrhenian Sea through the Corsica Channel, whereas to the west, it confines with the Catalan Sea. The circulation in the basin has been studied since the 1960s using hydrographic data and consists of a basin-wide cyclonic gyre (Ovchinnikov, 1966; Crepon et al., 1982), which extends over the upper 500 m and can spread out to the west into the Catalan Sea. In the Corsica Channel, the northward-flowing Eastern Corsican Current (ECC) brings Tyrrhenian water into the Ligurian Sea. West of Corsica another northward current prevails (the Western Corsican Current; WCC), which is part of the large cyclonic circulation. Previous works demonstrated the existence of seasonal variability of currents in the eastern Ligurian Sea. A stronger seasonal signal was observed in the Corsica Channel than in the WCC, with the warmer ECC being more energetic in winter and spring than in summer (Astraldi and Gasparini, 1992). The confluence of the ECC and the WCC north of Corsica forms the Northern Current (NC), also called the Liguro-Provençal-Catalan Current, which flows along the Italian (west of Genoa), French and Spanish coasts (Millot, 1991). Within the NC currents can reach 1 m s^{-1} at the surface (Poulain et al., submitted for publication) and about 5 cm s^{-1} at 400 m depth. Its core is narrow and centered at 20 km or less from the shore in spring-summer, whereas it is broader and more distant from the coast in autumn (Sammari et al., 1995).

Numerical simulations (Herbaut et al., 1997; Mounier et al., 2005; Barth et al., 2005) demonstrated that the WCC, ECC and NC, and the overall cyclonic circulation, are actually thermohaline and wind driven. The cyclonic circulation is reinforced in winter by the wind stress curl acting over the basin and by the induced deep water formation. A significant seasonal variability is observed over the basin, with the winter cyclonic gyre being wider and more coherent, while the summer circulation is more fragmented, resulting in a closed recirculation structure in the Ligurian basin, and smaller recirculations and vortices linked to topography (Astraldi et al., 1994). Significant baroclinic instabilities are present, with deformation radius going from less than 10 km (Marullo et al., 1985) to about 20 km (Vignudelli et al., 2003).

2.2. Drifters

The data set used for this study derives from CODE drifters deployed as part of MREA field experiments in the Ligurian Sea. Most of the deployments involved clusters of 3–5 drifters with initial distances less than 1 km at a single location in the vicinity of the ODAS buoy (9° 10.2' E, 43° 47.4' N). One single cluster (#4 in 2007, see Table 1) was deployed further west, along the French coast, off Nice (Fig. 1). Deployments were carried out between May and July 2007 as part of the MREA07 and LASIE07 (Ligurian Air Sea Interaction) experiments (Fabbroni, 2009), and in October 2008 during the MREA08 experiment. The cluster characteristics are shown in Table 1. Further details on the data and on the mean flow analysis are given in Poulain et al. (submitted for publication).

CODE drifters have been developed by Davis (1985) in the early 1980s and are used to measure the currents in the first meter under the sea surface. The CODE drifters used in this study were manufactured by Technocean, model Argodrifter (more details in Poulain, 1999). In addition to the standard satellite Argos tracking and telemetry, the drifters were equipped with Global Positioning System (GPS) receivers, which has a higher accuracy (approx. 10 m), sampled every hour (see Barbanti et al., 2005). Both Argos and GPS data were quality controlled, combined and interpolated

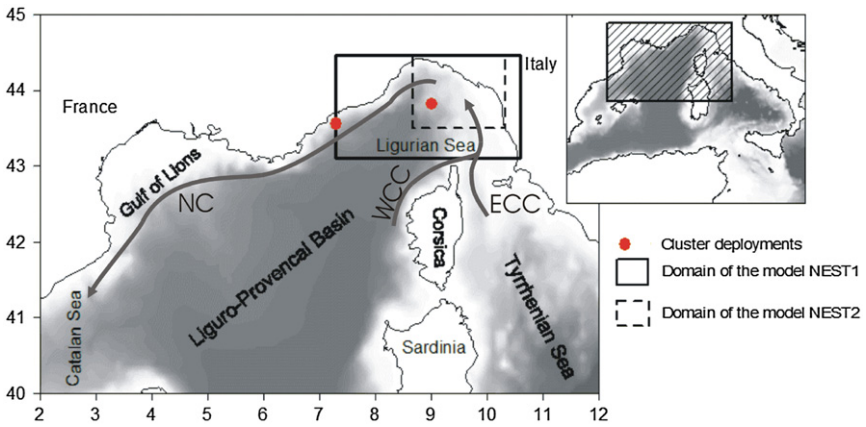

Fig. 1. Schematic of the Liguro-Provençal basin (the inset to the right shows its location in the north–west Mediterranean Sea) and main currents; NC: Northern Current, WCC: Western Corsican Current, ECC: Eastern Corsican Current. The red dots show the cluster launch positions and the two boxes show the two domains of the NCOM model. (For interpretation of the references to color in this figure legend, the reader is referred to the web version of this article.)

Table 1
Details on the cluster deployments conducted in the Ligurian Sea from the Italian Navy ships Galatea and Magnaghi and the Italian CNR ship Urania during the MREA07 and MREA08 experiments.

	Deployment date	Deployment longitude	Deployment latitude	No. drifters
2007 cluster ID				
1	May 14, 2007	9.232	43.851	5
2	June 17, 2007	9.157	43.894	5
3	June 22, 2007	9.089	43.851	5
4	July 17, 2007	7.356	43.594	4
2008 Cluster ID				
1	October 01, 2008	9.203	43.891	3
2	October 10, 2008	9.198	43.853	3
3	October 22, 2008	9.130	43.835	3

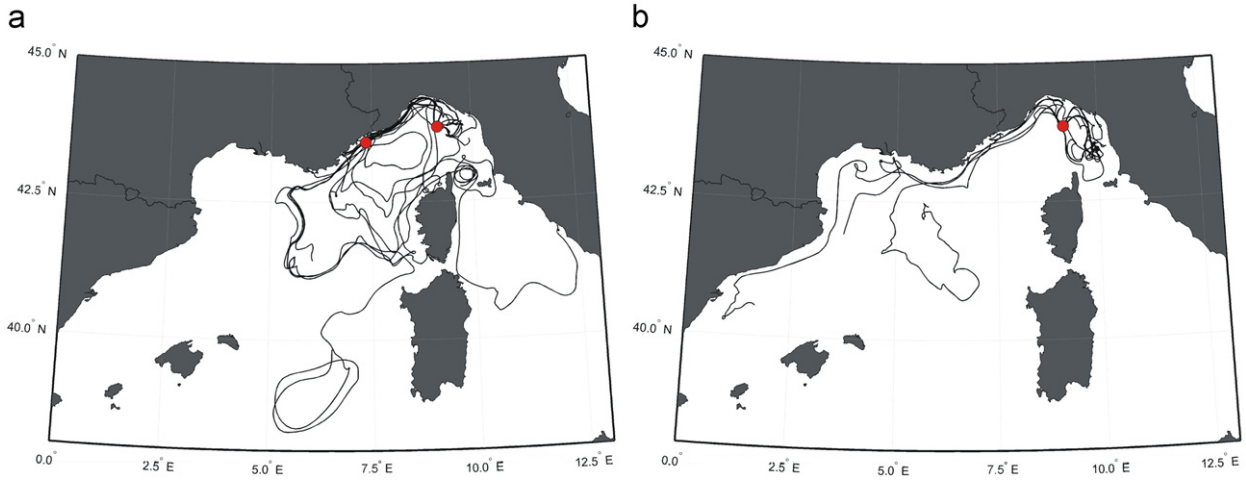

Fig. 2. Spaghetti diagrams of the drifters deployed during the (a) MREA07 and (b) MREA08 experiments. Red dots indicate the launch positions of the clusters. (For interpretation of the references to color in this figure legend, the reader is referred to the web version of this article.)

at 2-hour uniform intervals using the optimal interpolation method described in Hansen and Poulain (1996). They were subsequently low-pass filtered with a hamming filter (cut-off period at 36 h), in order to eliminate tidal and inertial variability, and then sub-sampled every 6 h. The influence of such filtering on the computed relative dispersion is investigated below.

In total, the data set consists of 28 individual trajectories spanning from May 2007 to January 2009. Drifter data from the MREA07 experiment lasted from 14th May 2007 to 19th October 2007. They are therefore considered representative of summer conditions, while those from the MREA08 experiment covered the period 1st October 2008–23rd January 2009 and are considered to sample fall-winter conditions. The drifters covered a relatively large area of the northwestern Mediterranean (Fig. 2a and b), and some units even escaped into the Tyrrhenian, Catalan and Algerian subbasins. Spatial coverage is maximal in the eastern Ligurian Sea north of Corsica, and in the NC between Genoa and the Gulf of Lions. Some drifters entered into the Gulf of Lions in 2008, before continuing towards the Catalan Sea (Fig. 2b).

The number of original drifter pairs in the data set is shown in Fig. 3 (upper panel) as a function of elapsed time since deployment. The total number of original pairs is 45, but they quickly decrease in time, especially after the first 10 days. MREA07 is characterized by a significantly higher number of pairs in deployment than MREA08, but the number decreases fast due to beaching and high mortality. The number of original pairs is also shown as a function of separation distance δ in Fig. 3 (middle panel), indicating that the majority of pairs is characterized by distances in the range between ≈ 500 m and 10–20 km. For comparison, we also show the total number of pairs versus δ (Fig. 3 (lower panel)) including original and chance pairs, i.e. pairs that approach one another at some time after the initial launch. The number of chance pairs is low at small scales, as it can be seen comparing Fig. 3 (middle panel and lower panel) for $\delta < 500$ m, but it increases significantly at increasing scales. The total number of pairs including chance ones is more than 50 in the range of 1–200 km.

2.3. Numerical model

Here, we also employ the velocity fields from the Navy Coastal Ocean Model (NCOM) model (Martin, 2000), that has been run in real time by the Naval Research Laboratory (NRL) during the MREA experiments. The NRL prediction system is based on the relocatable version of NCOM and it was configured with three nesting domains at resolutions of 4, 1.8, and 0.6 km, respectively, and forced by the COAMPS winds and NOGAPS0.5 thermal forcings. The nested models are run without data assimilation. The domains of the two inner nestings, used in this study, are shown in Fig. 1. The outermost nest is coupled with NCOM configured on a global scale at a 1/8° resolution which is operational at NAVO (http://www7320.nrlssc.navy.mil/global_ncom/index.html). For brevity, we refer the reader to Vandenbulcke et al. (2009) for further details on numerical models in MREA applications.

3. Analysis based on the observations

3.1. General description of the observations

In this section a general description of the velocity field as sampled by the drifters and of the typical behaviour of the clusters is given with the aim of providing a general framework for the

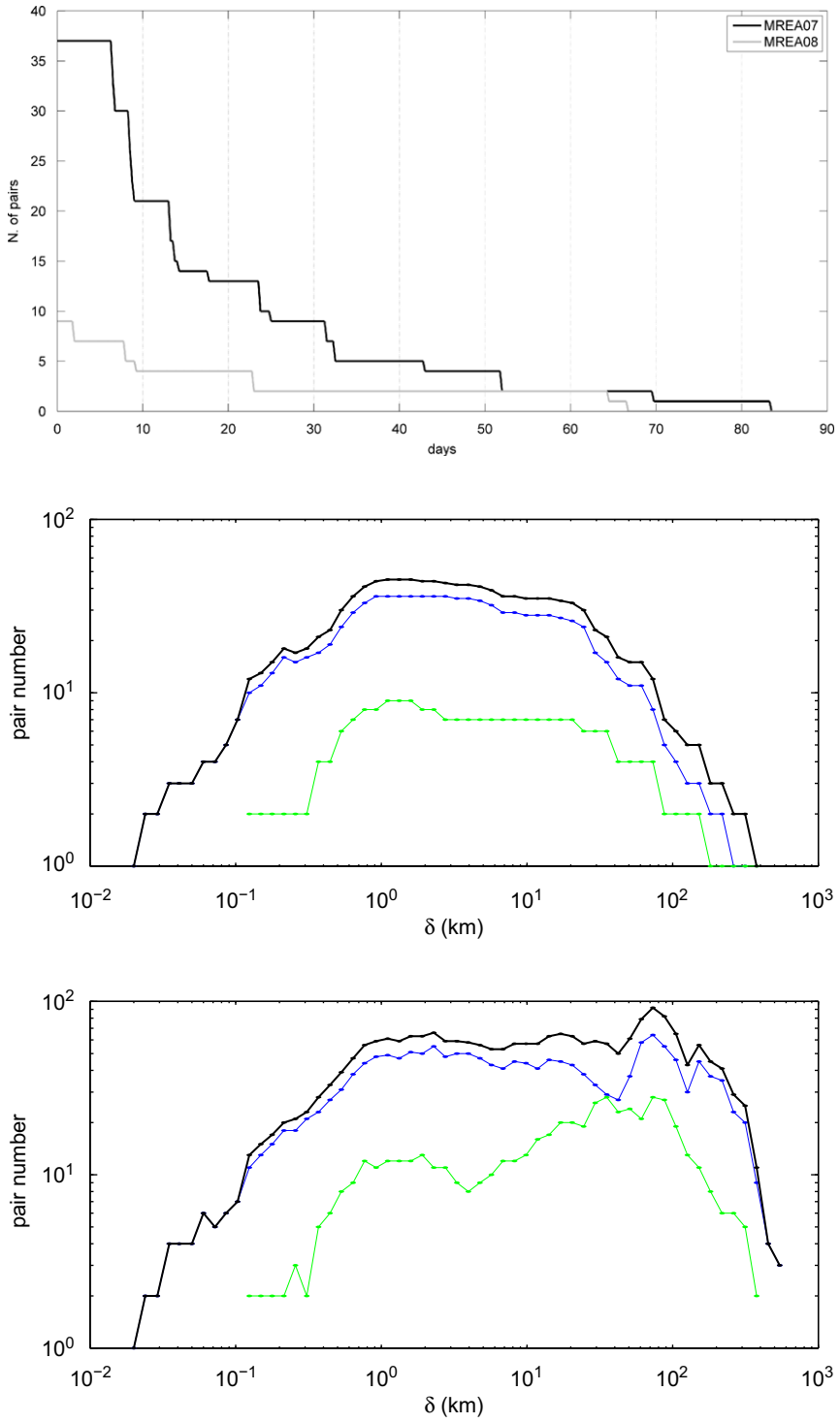

Fig. 3. (Upper panel) The number of original pairs as a function of elapsed time since deployment for MREA07 (black) and MREA08 (grey). (Middle panel) The number of original pairs as a function of separation distance δ for MREA07 (blue), MREA08 (green) and total data set (black). (Lower panel) Same as the middle panel but for chance pairs. (For interpretation of the references to color in this figure legend, the reader is referred to the web version of this article.)

interpretation of the relative dispersion statistics in the following sections.

In Fig. 4, velocity maps for the 2007 and 2008 data sets are shown, averaged in spatial bins of $0.25^\circ \times 0.25^\circ$, with a 50% overlapping between adjacent bins (only bins with more than four observations are shown). Note that these maps, as opposed to many other examples of binned fields from drifters present in the literature (Poulain, 2001; Bauer et al., 2002; Emery and Thomson, 2004), cannot be interpreted as representative of the stationary mean flow in the region, since there are not enough independent measures from the drifters. Rather, the maps in Fig. 4 should be interpreted as a visualization of the velocity field along drifter trajectories, i.e. of the average velocity as sampled by the drifters during their journey.

For both data sets, the NC and the general cyclonic circulation characteristics of the Liguro-Provençal basin can be recognized. While a closed cyclonic gyre can be seen in the Ligurian Sea in the 2007 data set (Fig. 4a), the 2008 drifters appear to move more towards the southwest on the continental slope eventually

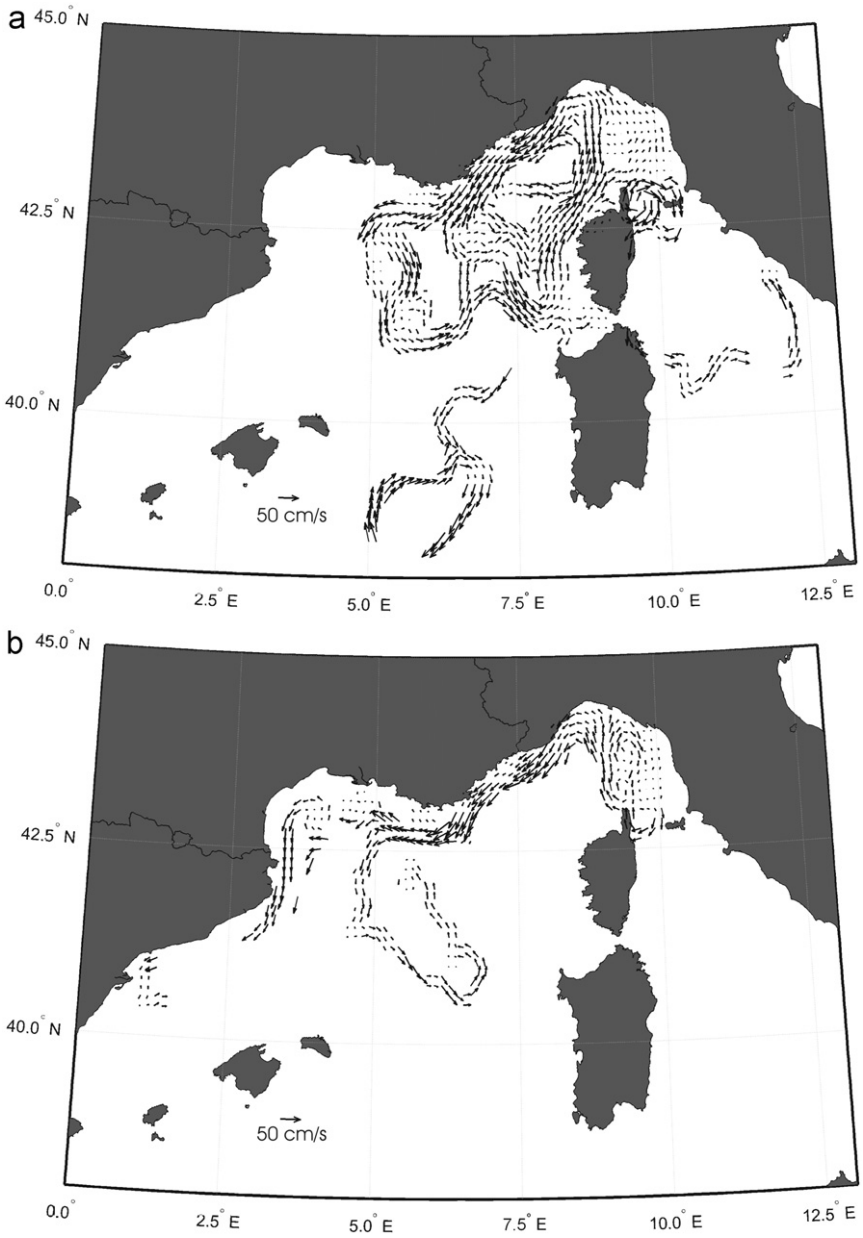

Fig. 4. Velocity field along trajectories in (a) 2007 and (b) 2008.

entering the Gulf of Lions before proceeding toward the Catalan Sea (Fig. 4b). This difference is consistent with the general seasonal variability (Astraldi et al., 1994) discussed in Section 2.1. Further details on this aspect and on the physical response of the upper ocean to different types of wind regimes occurring during the measurements are discussed in Poulain et al. (submitted for publication). Here, we focus mostly on the velocity structures revealed by the drifters that will be relevant to our further discussion of relative dispersion. We notice that, in addition to the main cyclonic circulation, there are a number of mesoscale semi-permanent recirculations with radius of ≈ 20 km. The most prominent one is the anticyclone between the Corsica and Elba islands, that is especially clear in 2007 (July–August), with one drifter trapped and turning around five times. One would expect a similar feature especially during summer, a season of reduced Tyrrhenian outflow (Astraldi et al., 1990), but the recirculation was observed also in 2008 (November), even though in this case the drifter was trapped only for half a circle, before escaping toward the north. Other anticyclonic recirculations can be seen more to the north in front of the Italian coast at $\approx 9^{\circ}$E, 44°N, where the NC appears to bifurcate in 2008 (October–November), and for both data sets along the French coastal current. Finally, another interesting feature evident in both data sets is the presence of a less energetic area in the shallower eastern Ligurian Sea ($>9^{\circ}$E, $>43^{\circ}$N). Here the velocities are rather low when compared to those observed within the basin-scale gyre, and once there, drifters tend to be trapped. It is worth notice that this low-energy regime appears more pronounced during the summer data set of 2007, than during the fall-winter data set of 2008, as one would expect from previous studies (Astraldi et al., 1990).

Most of the clusters show a typical behaviour characterized by the example in Fig. 5a. The drifters are initially caught in the NC, and they move coherently following the current during the first few days after the launch, slowly separating. When the separation reaches a critical value of about 20 km (after approximately 3–8 days), the drifters abruptly separate. Only two of the clusters (#1 in

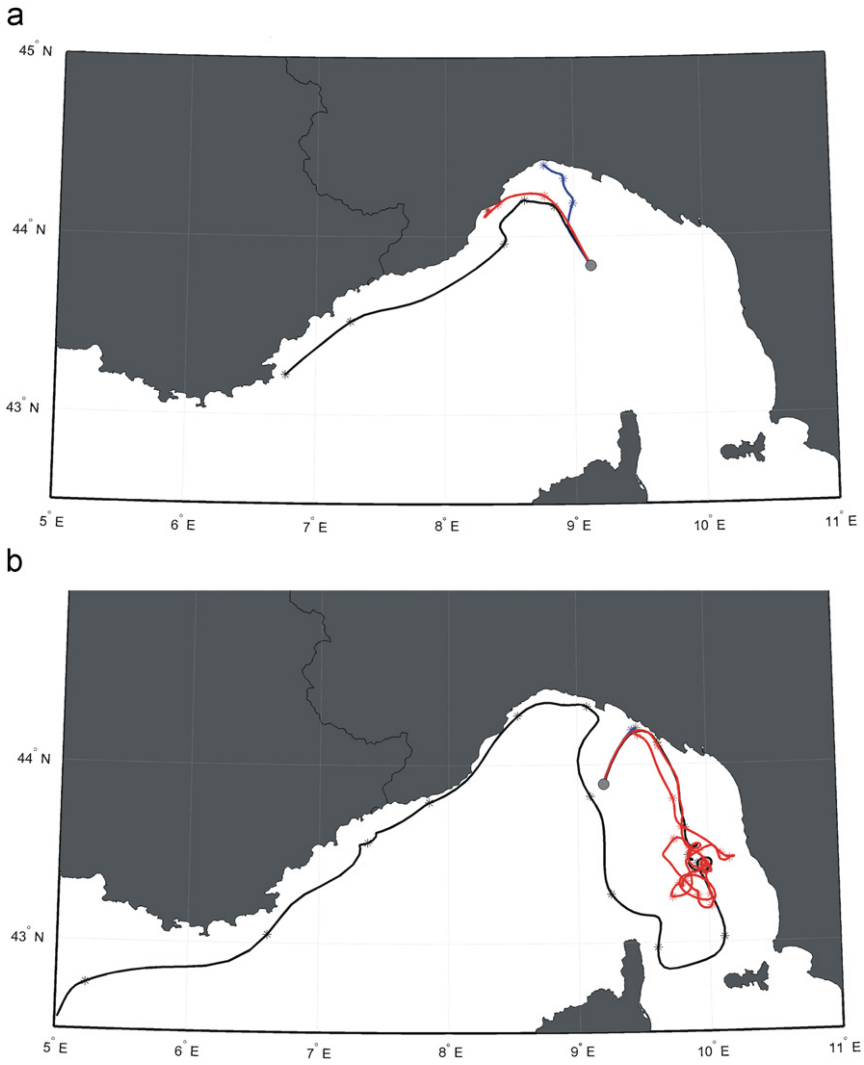

Fig. 5. Trajectories of cluster (a) #3 in 2008 and (b) #1 in 2008, to illustrating two extreme cases of cluster behaviour. The deployment location is the same, three weeks apart (1st October 2008 and 22nd October 2008). Asterisks are put along the single tracks every three days.

2007 and 2008) show a markedly different qualitative behaviour, illustrated in Fig. 5b. In these cases, at least one pair of drifters is trapped in the low-energy shallow eastern region. These drifters move slowly and no sudden and definite separation is observed. Rather, they tend to move almost randomly, separating and then getting closer again, so that after 20 days their average distance is still less than 20 km. Also, the drifters tend to be trapped in the area, and they are not easily re-entrained in the main current.

The trapping effect can be visualized computing maps of drifter-day data at successive times, as shown in Fig. 6 (for 2007) and Fig. 7 (for 2008). The number of drifter-days is binned as for the computation of the mean flow ($0.25^\circ \times 0.25^\circ$ bins with a 50% overlapping) and for time intervals of 1 week: the first 7 days after release are shown in (a), from day 7 to day 14 in (b), from day 14 to day 21 in (c), and from day 21 to day 28 in (d), for each year, respectively. We notice that drifter-days decrease over time, given that drifters die over the time intervals. Nevertheless, the results are expected to provide at least a useful qualitative information. The plots show that drifters entrained in the main NC are quickly advected, covering different parts of the basin in the different time intervals and showing an overall decrease in the concentration values: in other words, the data concentration appears to spread out in time over a broader area. On the other hand, in both years, a nucleus with maximum concentration can be observed persisting in time up to the last days in the eastern low energy area, south-east of the deployment point. This indicates that drifters are indeed efficiently trapped in the area.

3.2. Relative dispersion

To examine relative dispersion, we use mean particle pair separation and FSLEs. The information obtained by each method is then compared with the NCOM simulation results in Section 4.

Relative dispersion is computed from Eq. (1) using the original pairs. The initial distances between drifters in the clusters are less than 1 km, and at those scales the number of additional chance pairs is irrelevant (see Fig. 3 (middle panel and lower panel)). In Fig. 8a, the estimates of relative dispersion $D^2(t)$ are shown. Given the significant difference in seasonality and circulation in the 2007 and 2008 data sets, we have computed $D^2(t)$ separately for the two years, even though the number of pairs is limited especially for 2008. In Fig. 8b, a zoom of the first 10 days of $D^2(t)$ is shown for the 2007 and 2008 data sets, together with the values of the 95% confidence intervals (CI) characterizing the errors for each data set. We remark that the CIs might provide an underestimate of the error, given that the separation distribution is likely to be not Gaussian. The CIs for 2007 and 2008 do not overlap in the period between ≈ 2 and 6

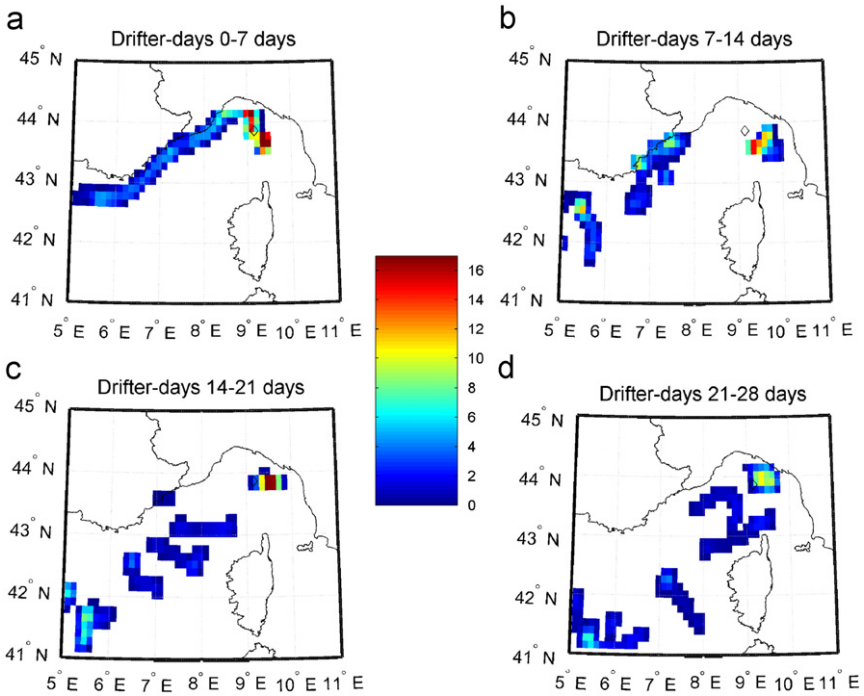

Fig. 6. Maps of drifter-days in 2007 in temporal bins of 7 days: (a) 0–7 days, (b) 7–14 days, (c) 14–21 days, and (d) 21–28 days.

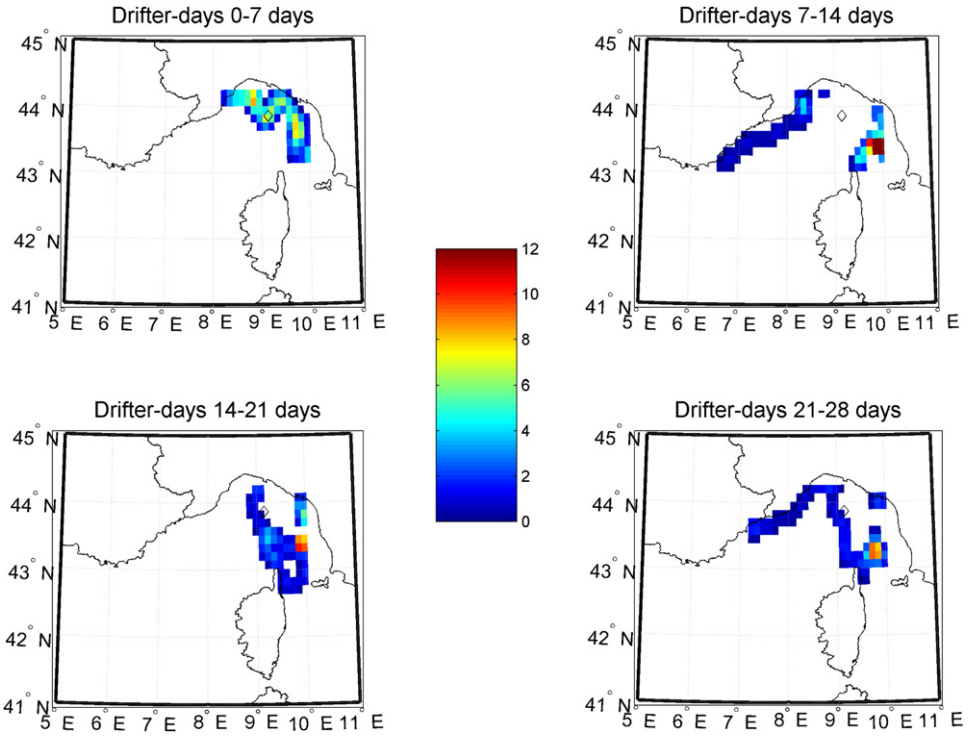

Fig. 7. Same as Fig. 6, but for 2008.

days, suggesting that the difference between the two data sets is at least partially significant. In order to illustrate the variability among the various launchings, we show $D^2(t)$ for the individual clusters in 2007 (Fig. 8c) and 2008 (Fig. 8d). As it can be seen, two of the 2008 clusters are very similar, while the third one has a very different behaviour. We will come back on this point in the following.

In the semi-log plots of the average $D^2(t)$ in Fig. 8a and b, an initial exponential phase of relative dispersion can be observed, appearing as an initial straight line. This is quantified in Fig. 9, where a linear fit is performed on (a) the two data sets combined and (b) the 2007 and 2008 data sets separately. The fit of the combined data set gives a linear dependency for the first 6.25 days with an *e*-folding time scale T_D of approximately 1 day (T_D=0.85

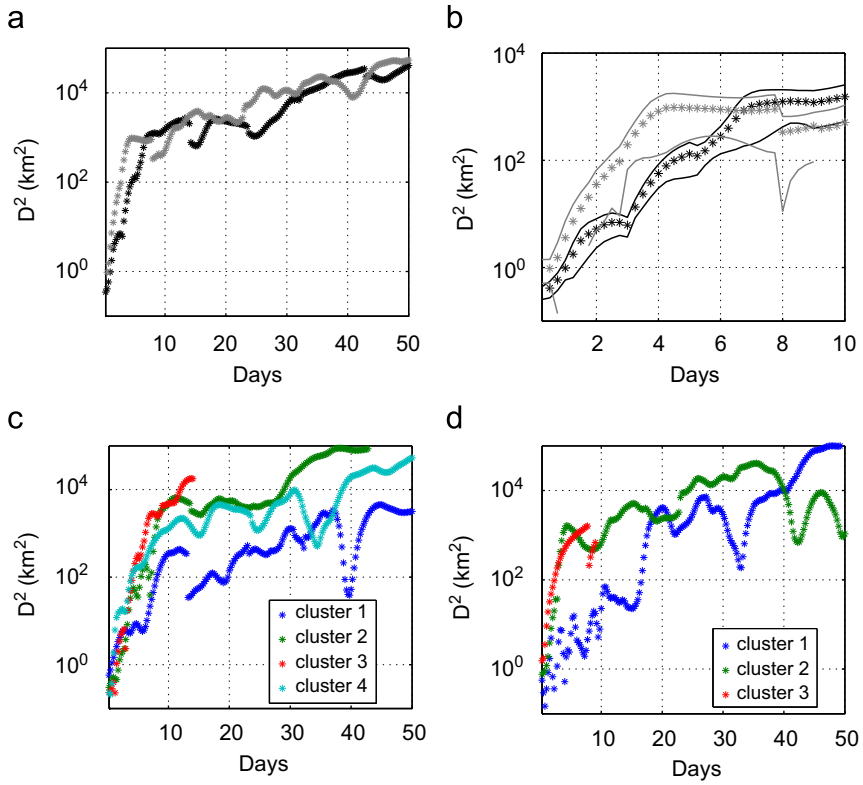

Fig. 8. Relative dispersion as a function of time, $D^2(t)$, in a semi-log plot for (a) all drifter pairs in 2007 (black symbols) and in 2008 (grey symbols). (b) The same as (a) but only for the first 10 days and with the 95% confidence intervals (in black lines for 2007 and grey lines for 2008). (c) $D^2(t)$ for single clusters in 2007 and (d) single clusters in 2008.

days). Similar results are obtained for the (dominant) 2007 data set, where the linear fit holds for 7.25 days with $T_D=0.87$ days, while for 2008 the linear dependency is found for 4.25 days and with a shorter e-folding time scale of approximately 1/2 day ($T_D=0.54$ days). Notice that the fits for the 2 years appear significantly different, as indicated by the error estimates in Fig. 9b. In terms of space scales, for both data sets the exponential growth occurs up to 25–35 km, more precisely between 1 and 35 km in 2007 and between 1.5 and 26 km in 2008. A clear regime change occurs after that but it is difficult to define the nature of the second regime because of the reduced number of data. The dispersion curve for the combined data set is also plotted in a log–log graph (Fig. 10) which suggests a power low dependence at times longer than $\approx$20 days, $D^2(t)\sim t^a$, with a power $2\leq a\leq 3$, even though the errors are quite high for a quantitative assessment.

Motivated by the model-based findings of Haza et al. (2008) and Poje et al. (2010) that spatial or temporal filtering of the velocity fields can have an influence on relative dispersion in the sub-mesoscale range, the same relative dispersion computations are repeated using the unfiltered drifter trajectory data with 2 h intervals. No difference from the above results has been found. This is because when dealing with oceanic drifters, the cumulative effect of all turbulent motions in the ocean acting on the drifters is fully represented, and filtering has only a minor effect on the resulting particle separations. In contrast, when filtering is applied to velocity fields in a model, then there is a corresponding truncation of the turbulent motions, and these errors tend to accumulate as separation errors in particle positions.

Overall the results show statistically significant exponential behaviour in the initial phase, that extends for the first few days and for more than one order of magnitude in space scales starting from initial distances of less than 1 km. This is consistent with earlier results from LaCasce and Ohlmann (2003) and Koszalka et al. (2009), who also find the initial exponential phase with an e-folding time of 2–3 days in the Gulf of Mexico and 0.5 day in the Nordic Seas. These results suggest that in the sub-mesoscale range relative dispersion is caused by nonlocal dynamics, and is likely to be dominated by the presence of the long-lived mesoscale structures, rather than by weaker, smaller and transient sub-mesoscale motions.

In order to have a better physical insight, it is useful to consider the plots of $D^2(t)$ for each cluster (Fig. 8c and d for 2007 and 2008, respectively). Even though the individual curves are not statistically significant because of the reduced number of data, it is clear that most of the clusters show a qualitative behaviour similar to the average ones (Fig. 8a and b) in the initial phase characterized by the exponential. From the trajectory point of view, they correspond to the clusters characterized by the classical behaviour in Fig. 5a, in that they are entrained in the cyclonic current and in its recirculations, and they move coherently until they reach a certain separation distance. It is interesting to notice, though, that two clusters appear to deviate quite clearly from the initial exponential behaviour. They are the same clusters (#1 in 2007 and 2008, see Table 1) that we have already discussed in Section 3.1 and that are characterized by pairs that separate slowly and are trapped in the less energetic region in the eastern Ligurian Sea (trajectories as in Fig. 5b). This suggest a possible different regime in this region, that may need further investigation with adequate drifter resources in the future.

3.3. Finite Scale Lyapunov Exponents (FSLEs)

Another metric related to relative dispersion is the FSLE introduced by Artale et al. (1997) and Aurell et al. (1997):

$$\lambda(\delta)=\frac{\ln(\alpha)}{\langle\tau(\delta)\rangle}, \tag{2}$$

where $\langle\tau(\delta)\rangle$ is the averaged time (over the number of particle pairs) required to separate from a distance of δ to $\alpha\delta$. This follows if

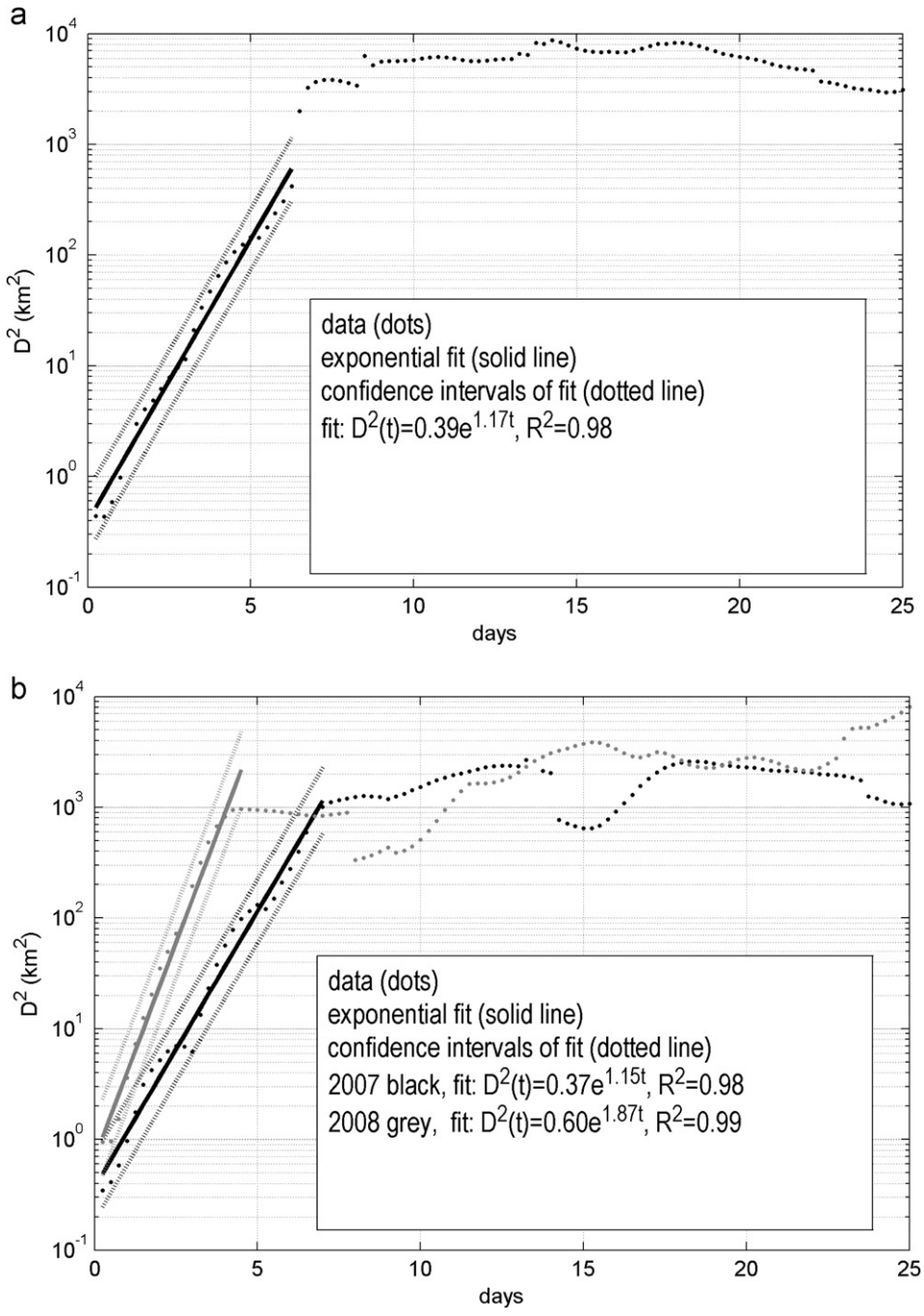

Fig. 9. Log–linear plots of $D^2(t)$ for (a) the combined data set, (b) the separated data sets: 2007 (black) and 2008 (grey). The linear fits are shown as solid lines. For the combined data set $D^2(t) \sim \exp(2\lambda_D t)$ with $\lambda_D = 0.58$ days^{-1} (or T_D=0.85 days, where $T_D = 1/(2\lambda_D)$ is the e-folding time); $\lambda_D = 0.57$ days^{-1} (or T_D=0.87 days) for 2007, and $\lambda_D = 0.93$ days^{-1} (T_D=0.54 days) for 2008. For each fit the 95% confidence intervals on the values predicted by the fit are shown as dotted lines. R^2 is the correlation coefficient of the fit.

it is assumed that $D(t) = D(0)\exp(\lambda_D t)$ (or $D^2(t) = D^2(0)\exp(2\lambda_D t)$), then $\lambda_D = \ln\{D(\tau)/D(0)\}/\tau$. The FSLE allows to isolate the contribution of dynamics at different space scales to particle separation, even though as for D^2 also FSLE necessarily averages over different types of spreading (hyperbolic or elliptic) that might occur in the domain. FSLE is not only more robust with respect to the average $D^2(t)$ at large scales that are typically dominated by those particles with largest separations (thus also small pair numbers), but also it highlights somewhat better the behaviour at the sub-mesoscale range, which is one of the areas of interest in the present study.

The spatial maps of the FSLE and related metric, the Finite-Time Lyapunov Exponent (FTLE, Haller, 1997), are employed increasingly more often in the Lagrangian analysis of oceanic flow fields (d'Ovidio et al., 2004; Olascoaga et al., 2006; Haza et al., 2007, 2008, 2010; Shadden et al., 2008; Poje et al., 2010). This is because spatial maps of the FSLE (and FTLE) are found (e.g. Molcard et al., 2006) to be accurate and computationally efficient proxies for the Lagrangian coherent structures (LCS). LCS are material surfaces controlling transport, that have been traditionally estimated on more complex algorithms centered around the identification of so-called hyperbolic trajectories (Ottino, 1989; Haller and Poje, 1998; Poje and Haller, 1999; Coulliette and Wiggins, 2000; Miller et al., 2002; Wiggins, 2005). Being a metric for relative dispersion, the spatial maps of FSLE would identify all mechanisms causing two-particle dispersion, namely not only dispersion due to hyperbolicity induced by nearby coherent structures (eddies and jets),

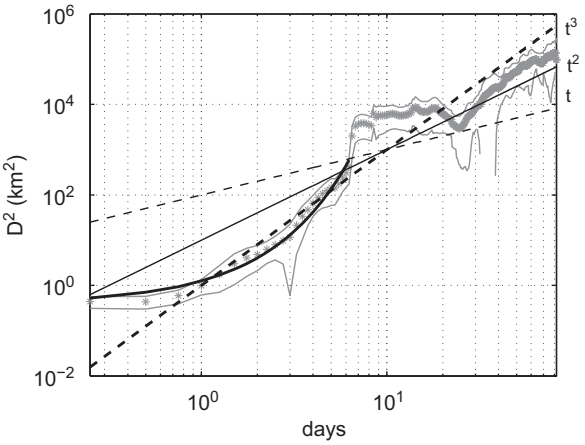

Fig. 10. Relative dispersion as a function of time in a log–log plot for all drifter pairs (the combined data set) in grey symbols. The thin grey lines represent the 95% confidence intervals. Curves corresponding to the initial exponential fit (thick black solid line), the diffusive regime $D^2 \sim t$ (thin black dashed line), ballistic regime $D^2 \sim t^2$, (thin black solid line), and Richardson regime $D^2 \sim t^3$ (thick black dashed line) are plotted in the background.

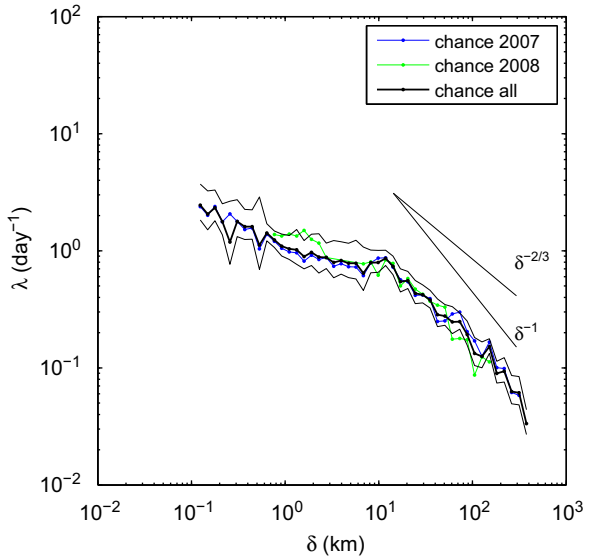

Fig. 11. The Finite Scale Lyapunov Exponent $\lambda(\delta)$ from chance pairs in 2007 (blue), 2008 (green) and the combined data set (black). The 95% confidence intervals CIs for the combined data set are shown in black thin lines. The slopes corresponding to ballistic $\lambda \sim \delta^{-1}$ and Richardson $\lambda \sim \delta^{-2/3}$ regimes are marked. (For interpretation of the references to color in this figure legend, the reader is referred to the web version of this article.)

but also due to shear dispersion and convergence/divergence zones due to three-dimensionality. Here, we employ the scale-dependent FSLE, which serves to isolate the different dispersion regimes corresponding to the different scales of the oceanic flows.

Three specific implementation details follow. The first relates to the choice of α in (2). Given the goal of examining the scale dependence of the relative dispersion as a function of spatial velocity resolution, we have chosen the smallest possible α in order to observe the finest possible scale dependence. As explained in Haza et al. (2008, Fig. 2b and Section 4.1), temporal resolution of trajectory data and statistical considerations impose a lower bound on the value of α. Specifically, α must not be chosen so small that pair separations occur at times smaller than the time increment of the available data. With these considerations in mind, we have chosen $\alpha = 1.2$. This parameter choice is consistent with Rivera and Ecke (2005) and slightly smaller than typical values ($\alpha = \sqrt{2}$) (Aurell et al., 1997; Lacorata et al., 2001; LaCasce and Ohlmann, 2003). Tests with $\alpha = 1.4$ and 1.7 show no significant difference with respect to the results discussed below.

The second issue relates to the computation of the scale-dependent FSLE using original or chance pairs. Original pair sampling is typically more accurate and readily feasible in the context of numerical models since it is based on particles launched together at a particular distance. Chance pairs are typically employed in the analysis of real drifters in which only a limited number of resources are available. Chance pair computation can sometimes lead to a misrepresentation of the exponential regime at the sub-mesoscale range as drifters may tend to preferentially sample certain flow regions (e.g. Fig. 4c in Haza et al., 2008). Here we use chance pairs to have a somewhat better coverage at different separation scales for FSLE computation using drifter data. Below we also perform a specific investigation on the impact of using chance versus original pairs results from the NCOM model.

Third, so-called fastest-crossing method is used to compute FSLE. For the purpose brevity, we refer the reader to Poje et al. (2010, p. 44 and Fig. 17) for a more detailed discussion.

The scale-dependent FSLE $\lambda(\delta)$ (Fig. 11) is computed on the basis of original and chance pairs separately for the clusters released in 2007 and 2008. In addition, we also computed FSLE for the entire data set (independent of their launch time). As shown in Fig. 3 (lower panel), the total data set shows more than 50 pairs in the separation range of approximately 0.7 km $\leq \delta \leq$ 200 km, thus this δ range has the highest reliability. Error estimates for the entire data set are also shown in Fig. 11, in terms of 95% CIs, even though as already remarked in Section 3.2 CIs might underestimate the errors since they are based on a Gaussian distribution hypothesis that is likely not to hold. Only estimates with more than 10 pairs are considered. Based on Fig. 11, we note that there is no significant difference between the FSLE curves obtained from the 2007 and 2008 clusters. In particular, we find an exponential regime (approximately scale-independent FSLE value, or FSLE "plateau") characterized by 0.7 day^{-1} $\leq \lambda \leq$ 1 day^{-1} for 1 km $\leq \delta \leq$ 10 km. At smaller scales, namely for 0.1 km $\leq \delta \leq$ 1 km, λ seems to gradually increase to about 2 day^{-1}. Nevertheless, there is a significant reduction in the number of pairs at such small scales and these numbers may contain sampling errors.

Table 2
Lyapunov exponents computed from curve fitting with $D^2(t) \sim \exp(2\lambda_D t)$ and the limiting value of $\lambda_{max}(\delta)$ for CODE drifters in MREA experiments.

Year	λ_D	λ_{max}
2007	0.57 days^{-1} for $t \leq 7$ days	0.7–1.0 days^{-1} for 1 km $\leq \delta \leq$ 10 km
2008	0.93 days^{-1} for $t \leq 4$ days	0.7–1.5 days^{-1} for 1 km $\leq \delta \leq$ 10 km

These estimated limiting values of relative dispersion are reasonably consistent with λ_D obtained on the basis of $D^2(t)$ in Section 3.2, using $\lambda_D = 1/(2T_D)$. The estimates of λ_D from $D^2(t)$ give values of 0.57 day^{-1} for 2007, 0.93 day^{-1} for 2008 and 0.58 day^{-1} for the combined data sets (Table 2). The range is similar for the FSLE plateau, that gives $\lambda \approx 0.7-1.5$ day^{-1}. At a more detailed level, we note that there is virtually no significant difference between 2007 and 2008 in the FSLE, as opposed to a factor of about two that is derived from relative dispersion $D^2(t)$. Given the low pair numbers for the 2008 data set (essentially less than 10), it is possible that estimates from two different methods did not quite converge. Another difference between the results of the $D^2(t)$ and FSLE metrics is that the exponential range extends to more than 20 km for $D^2(t)$ (also for the combined data set) and to approximately 10 km for FSLE. Similar differences have been previously found in the analysis of other data sets. As discussed by LaCasce and

Ohlmann (2003) they can be due to different sampling (chance versus original pairs), the use of different independent variables in the two metrics, or simply errors due to the sparse sampling.

To our knowledge, MREA07-08 experiments contain only the third cluster data set that allows computation of relative dispersion at the sub-mesoscale range and indicate a clear exponential regime. In comparison, a limiting FSLE value of $\lambda_{max} = 0.3$ days^{-1} for $\delta < 20$ km and $D^2(t)$ e-folding time of 2 days (or $\lambda_D = 0.25$ days^{-1}) were computed from SCULP drifters (up to 140 pairs) in the Gulf of Mexico (LaCasce and Ohlmann, 2003), and $D^2(t)$ e-folding time scale of roughly half a day (corresponding to $\lambda_D \approx 1$ day^{-1}) at spatial scales less than 10 km from POLEWARD drifters (up to 67 pairs) in the Nordic Seas (Koszalka et al., 2009). Published values computed from realistic models are $\lambda_{max} \approx 0.6$ days^{-1} for $\delta < 10$ km from NCOM with 1 km horizontal resolution configured in the Adriatic (Haza et al., 2008), and $\lambda_{max} \approx 0.4$ day^{-1} for $\delta < 50$ km from HYCOM configured in the North Atlantic with 8 km horizontal resolution (Poje et al., 2010).

Nevertheless, two important differences from previous findings should be emphasized regarding the sub-mesoscale range. The first is that Lumpkin and Elipot (2010) find values exceeding $\lambda_{max} \approx 10$ day^{-1} at scales $\delta < 3$ km on the basis of CLIMODE drifters near the Gulf Stream region. These measurements are interesting not only because of such differences from the above values (up to 33-fold), but also because no exponential regime was identified. Both the high λ_{max} and the lack of an exponential regime can be possibly attributed to yet unknown reasons associated with their launch under severe wind (winter) conditions. Second, values of $4 \le \lambda_{max} \le 7$ day^{-1} at scales $\delta < 1$ km have been obtained for the exponential regime in the Gulf of La Spezia using VHF radar velocity fields (Haza et al., 2010). This value is also significantly higher than the others, possibly because of the small size of this Gulf (with Rossby number of approximately 1) and its complex geometry and forcing flow patterns different than those in the open ocean.

For 10 km $< \delta \le 200$ km, namely in the mesoscale range, a power law behaviour is obtained with $\lambda(\delta) \sim \delta^{-0.75}$ (Fig. 11), which is in the middle of Richardson ($\delta^{-2/3}$) and ballistic (δ^{-1}) regimes. Unlike the dispersion in the sub-mesoscale range, mesoscale dispersion is less controversial. LaCasce and Bower (2000) observed Richardson dispersion from sub-surface floats in the western Atlantic, Ollitrault et al. (2005) found indication for Richardson regime from sub-surface floats in both western and eastern Atlantic, while Lumpkin and Elipot (2010) arrived at Richardson's law at a very wide scale range of 1–3 to

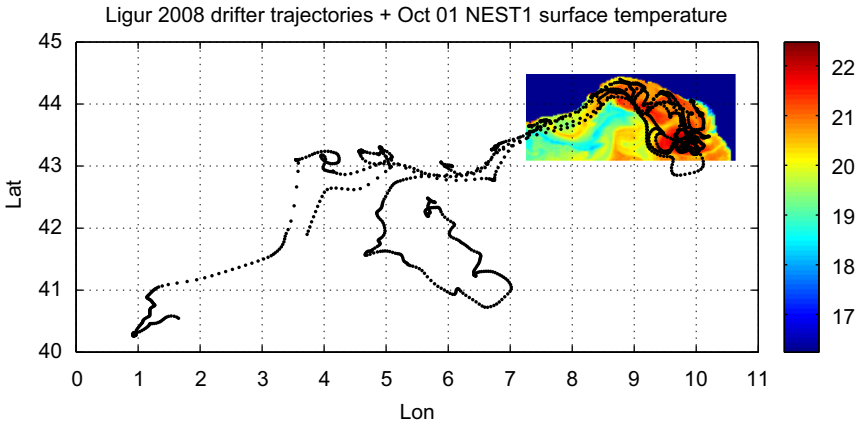

Fig. 12. MREA08 CODE drifter trajectories superimposed on sea surface temperature from nest1 on October 1, 2008.

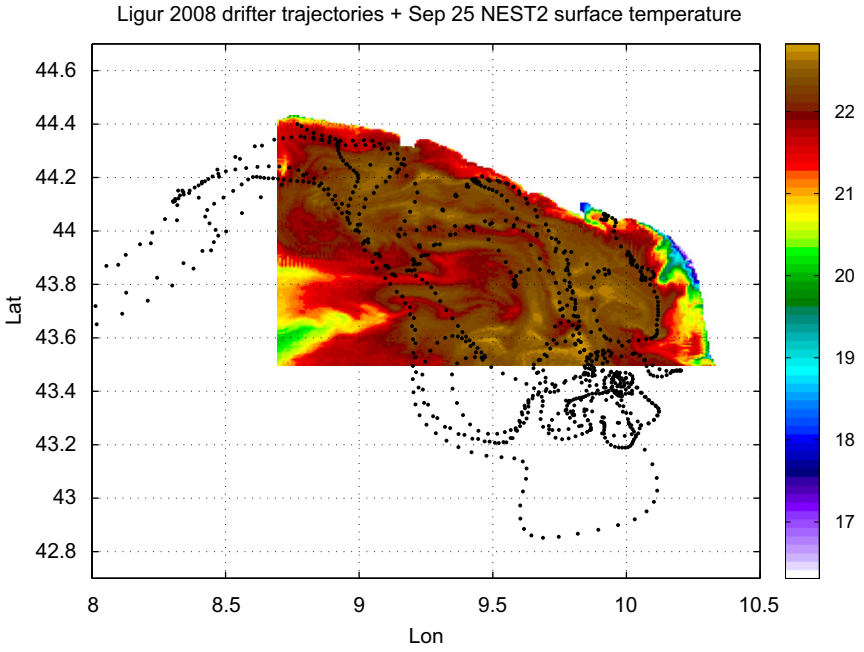

Fig. 13. MREA08 CODE drifter trajectories superimposed on sea surface temperature from nest2 on September 25, 2008.

300–500 km from surface drifters. Koszalka et al. (2009) report Richardson behaviour for spatial scales of 10 to roughly 100 km (and temporal scales of 2–10 days) from POLEWARD drifters, while LaCasce and Ohlmann (2003) find a similar power law for separation scales of approximately 30–300 km in the Gulf of Mexico. Richardson regime is also identified in realistic numerical simulations in the North Atlantic using HYCOM for temporal scales longer than two days and spatial scales larger than 200 km (Poje et al., 2010). An intermediate regime between Richardson and ballistic ($\lambda(\delta) \sim \delta^{-0.8}$) was found from a study based on NCOM in the Adriatic (Haza et al., 2008), where the western Adriatic current plays a prominent role in setting up a shear dispersion regime. Certainly, Figs. 6 and 7 indicate that MREA drifters entrain into and sample the Ligurian current well. As such, the mesoscale relative dispersion power law appears to reflect effects of shear dispersion (ballistic regime).

4. Analysis based on NCOM

Next, we proceed to employ the fields generated by NCOM operationally for the Ligurian Sea (Rixen and Coelho, 2007; Rixen et al., 2008) during a period overlapping with the drifter coverage, from 25 September 2008 to 9 October 2008. In particular, we address the following questions:

(a) Are relative dispersion statistics, $D^2(t)$ and $\lambda(\delta)$, from NCOM consistent with those obtained from CODE drifter clusters?
(b) Is there a difference between different model horizontal resolutions, 1.8 km (denoted nest1), and 0.6 km (denoted nest2) in that the latter is more realistic than the former?
(c) Can we quantify the effects of reduced sampling and chance pairs on relative dispersion statistics using synthetic data from the model?

In addition to these main questions, we also perform a preliminary investigation to verify whether or not any of the model configurations is able to capture a different flow regime in the shallow area in front of the Italian coast that was inferred from the observed drifters (Sections 3.1 and 3.2).

The computational domains, schematically shown in Fig. 1, are further illustrated in Figs. 12 and 13 showing also the observed trajectories. The domain denoted nest1 is shown in Fig. 12, while nest2 is depicted in Fig. 13. Clearly, both domains span smaller spatial scales than those covered by the CODE drifters. More specifically, nest1 (nest2) has a zonal extent of 260 km (132 km) and meridional extent of 148 km (108 km). Given their fine horizontal (1.8 and 0.6 km) resolutions, both domains cover a

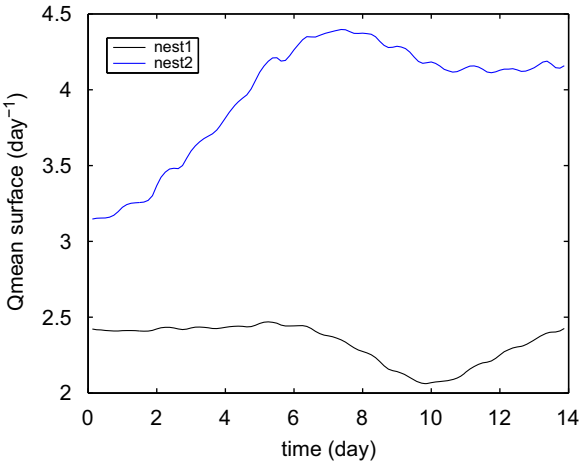

Fig. 15. Square root of the average positive Okubo–Weiss parameter as a function of time $\langle Q^+ \rangle(t)$ for both nest1 and nest2 domains.

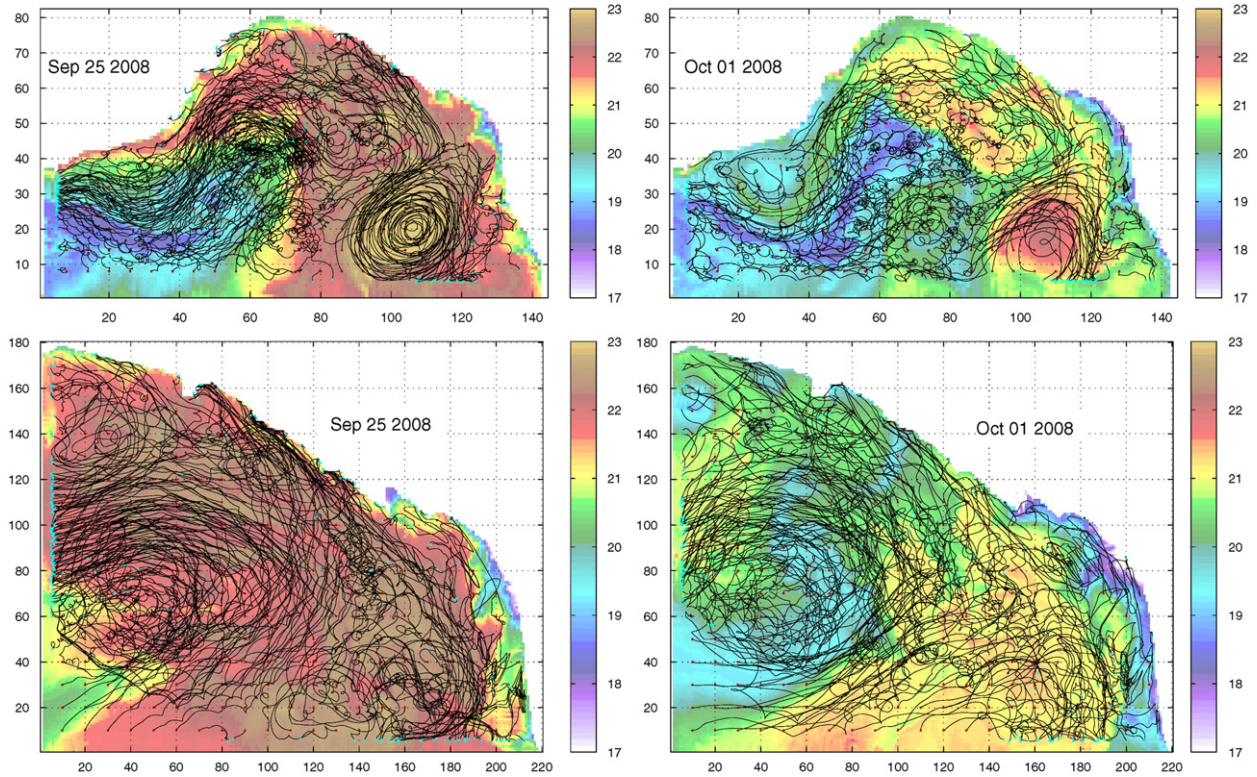

Fig. 14. Surface trajectories of synthetic particles advected using velocity fields from nest1 (upper panels) and nest2 (lower panels). Modeled surface temperature fields from 25 September 2008 (left panels) and 1 October 2008 (right panels) are superimposed.

sufficiently large range of scales overlapping both sub-mesoscale and mesoscale processes. In order to compute relative dispersion statistics, synthetic particles are launched in a cross-configuration (four satellite particles around the one centered at a grid point), where the center particle is released every three grid points in nest1 (5.4 km apart) and every five grid points in nest2 (3 km apart). This corresponds to a total of 3260 particles in nest1 and 4750 particles in nest2. The satellite particles are launched with distances of $r_0=0.1$, 0.5, 1, 2 and 5 km. The reason for these different configurations is to compute $\lambda(\delta)$ by sampling adequately in the sub-mesoscale range on the basis of original pairs, as opposed to relying on occasional chance pairs that converge to small distances. As shown below, these configurations maintain a high (about 2000–3000) pair density at the sub-mesoscale range. The particles are advected using a fourth-order Runga–Kutta method and linear subgrid interpolation scheme for the velocity field.

Subsets of the synthetic drifter trajectories are depicted in Fig. 14 for both model configurations. One of the pronounced features in nest1 is a large anticyclonic eddy in the southeastern part of the domain, which seems to be of questionable realism on the basis of the velocity field shown in Fig. 4, and prior observational studies of the region, as discussed above. Previous assessment of the model (Vandenbulcke et al., 2009) also indicates that while the model has a realistic energy level, the exact location of the structures may not have been accurately captured, as it can commonly happen in non-assimilating (free) runs in highly nonlinear regions. One of the implications of this eddy is to obscure the dynamically different flow field that seems to be evident on the basis of CODE drifters. In contrast, nest2 seems to be configured far too north with respect to the region identified for being possibly rich with sub-mesoscale motion. We conclude that these dynamics are not captured in the present set of NCOM simulations.

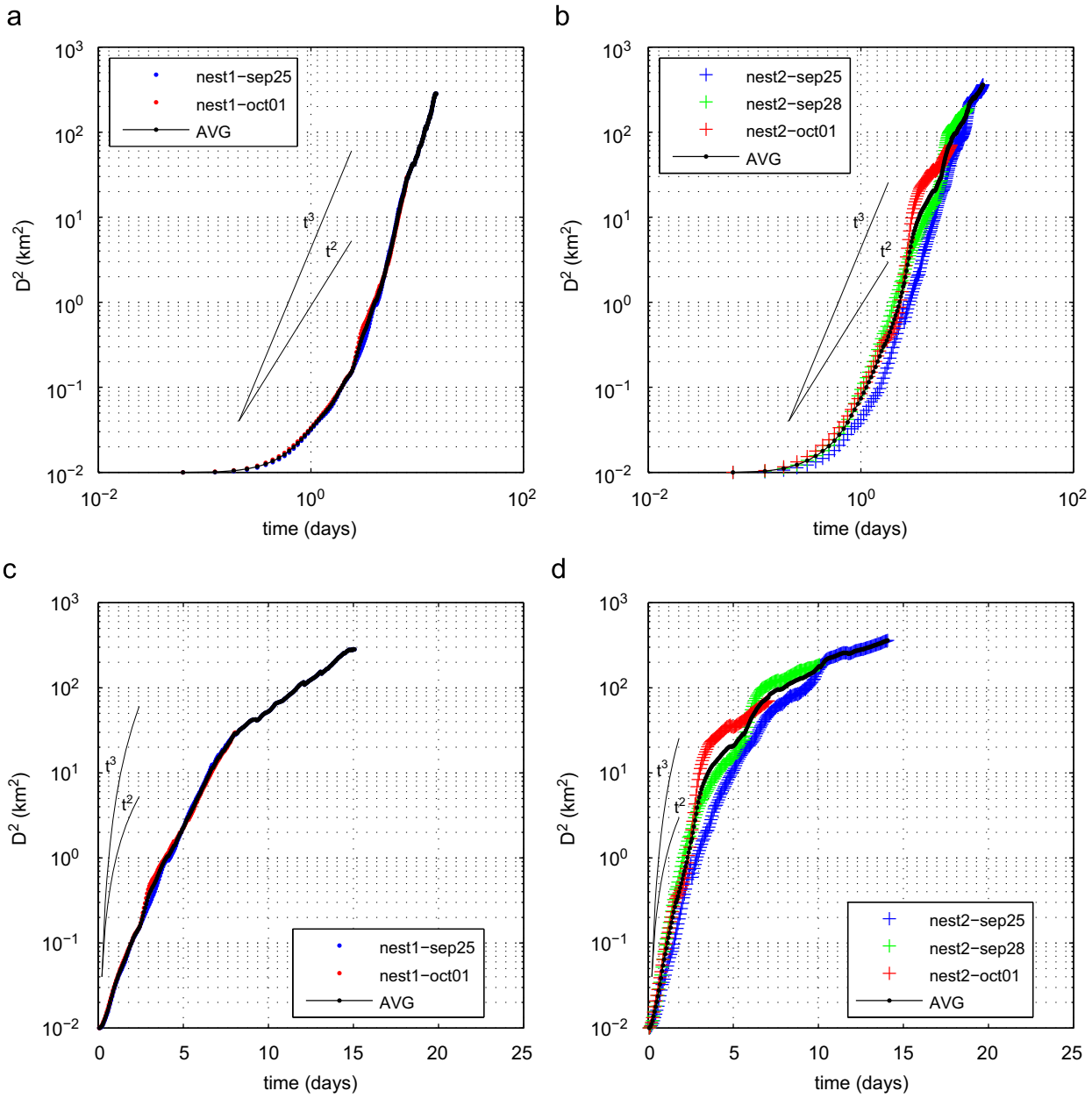

Fig. 16. Log–log plots of $D^2(t)$ from NCOM for (a) nest1 and (b) nest2 computed using $r_0=100$ m and starting from different initial dates (September 25, September 28 and October 1). (c), (d) Log–linear plots to identify the exponential regime over short periods. Curves corresponding to ballistic $D^2 \sim t^2$, and Richardson $D^2 \sim t^3$ are plotted in the background.

In order to get a sense of the difference between the velocity fields obtained from two resolutions, we compute a metric $\langle Q^+ \rangle$ defined as

$$\langle Q^+ \rangle = A^{-1} \int \sqrt{Q}\, dA \quad \text{for } Q > 0, \tag{3}$$

where A is the area of the computational domain, $Q = S^2 - \omega^2$ is the Okubo–Weiss criterion (Okubo, 1970; Weiss, 1991), $S^2 = (\partial u/\partial x - \partial v/\partial y)^2 + (\partial v/\partial x + \partial u/\partial y)^2$ is the square of the horizontal strain rate, and $\omega^2 = (\partial v/\partial x - \partial u/\partial y)^2$ is the square of horizontal vorticity. $\langle Q^+ \rangle$ is a measure of hyperbolicity in the velocity field and is shown to correlate well with the limiting value of the FSLE (Poje et al., 2010). The time evolution of $\langle Q^+ \rangle$ from both meshes (Fig. 15) shows that the finer mesh simulation is characterized by higher values than the coarser mesh simulation, which indicates higher resolved shears. This is common in numerical models (Poje et al., 2010) and implies higher limiting values for the FSLE.

Results for relative dispersion $D^2(t)$ for both nest1 and nest2 are shown in Fig. 16 starting from initial separation of 100 m and considering log–log (upper panels) and log–linear (lower panels) plots in order to better identify the exponential regime. Results from sampling starting at different dates (September 25, September 28 and October 1, 2008) are shown together with the average curve. They appear quite similar, especially for nest1. A linear fit is found to be valid up to 7 days for nest1 and up to 2.5–3 days for the average curve for nest2, with values of $\lambda_D \approx 0.58$ days^{-1} for nest1 and 0.92 days^{-1} for nest2 (see also Table 3). Regarding longer time scales, relative dispersion from nest1 is consistent with a ballistic regime for approximately 6 days $\leq t \leq 11$ days and Richardson regime for $t > 11$ days, while nest2 indicates Richardson regime for $t > 6$ days.

Several points can be made on the basis of these numbers. First, nest2 gives higher Lyapunov exponents than nest1, which is consistent with the higher resolved shears, as quantified by $\langle Q^+ \rangle^{1/2}$ in Fig. 15. Second, the values obtained from nest2 appear to be in good agreement with those from 2008 CODE drifters, while λ_D from nest1 is significantly (by up to 50%) smaller. Third, the results in nest2 show some sensitivity to the exact launch time in that λ_D can vary by about 25%. Finally, the exponential regime in nest1 and nest2 extends up to space scales of 3 km. Following Poje et al. (2010), exponential growth is expected to occur below the model resolution, but the fact that here the exponential growth persists above the model mesh spacing in nest2 indicates that it is indeed caused by resolved dynamical reasons.

Nevertheless, the range of the exponential regime in $D^2(t)$ from the model is significantly smaller than that from the drifter data. One possibility for this difference could be that real drifters sample high strain regions, whereas the model results are based on average of the nest2 domain. In order to explore the sensitivity of $D^2(t)$ on the sampling region, we have launched 2205 synthetic particles in regions close to the actual in situ drifter launches. The results show a significant variation in the extent of an exponential regime, ranging from approximately 6 or 7 km for September 25 and October 1 cases, to approximately 14 km for September 28 launches (Fig. 17).

The FSLEs are computed first from original pairs with $r_0 = 0.1$, 0.5, 1, 2 and 5 km, while the separation scales in between and larger than 5 km are computed from chance pairs. This calculation ensures high pair density across all δ. The results are shown in Fig. 18. A limiting FSLE value of $\lambda_{max} \approx 0.7$ days^{-1} is obtained for nest1 (Fig. 18a), while $\lambda_{max} \approx 1$ day^{-1} for nest2 (Fig. 18b). While there is a good agreement between the $\lambda(\delta)$ from NCOM nest1 and CODE drifters for $\delta > 10$ km, namely for the mesoscale range, the range of agreement improves down to $\delta > 1$ km in nest2. Given the model resolution, scales smaller than 1 km are not resolved. As such, both the model, due to unresolved dynamics, and observations, due to low pair density, contain errors for separation scales smaller than 1 km.

It is also noted that the FSLE curves from nest2 are shifting to higher Lyapunov exponents with smaller separations, while this does not happen in the FSLE curves from nest1 (Fig. 18b versus a).

Table 3
Lyapunov exponents computed from linear curve fitting to $D^2(t) \sim \exp(2\lambda_D t)$ and the limiting value of $\lambda_{max}(\delta)$ from NCOM 2008 output with nest1 and nest2 domains.

Domain/ resolution	λ_D	λ_{max}
nest1	0.58 days^{-1} for $t \leq 4$ days	0.7 days^{-1} from original pairs 1.0 days^{-1} from chance pairs
nest2	0.92 to 1.15 days^{-1} for $t \leq 2$ days	1 days^{-1} for original pairs 2 days^{-1} from chance pairs

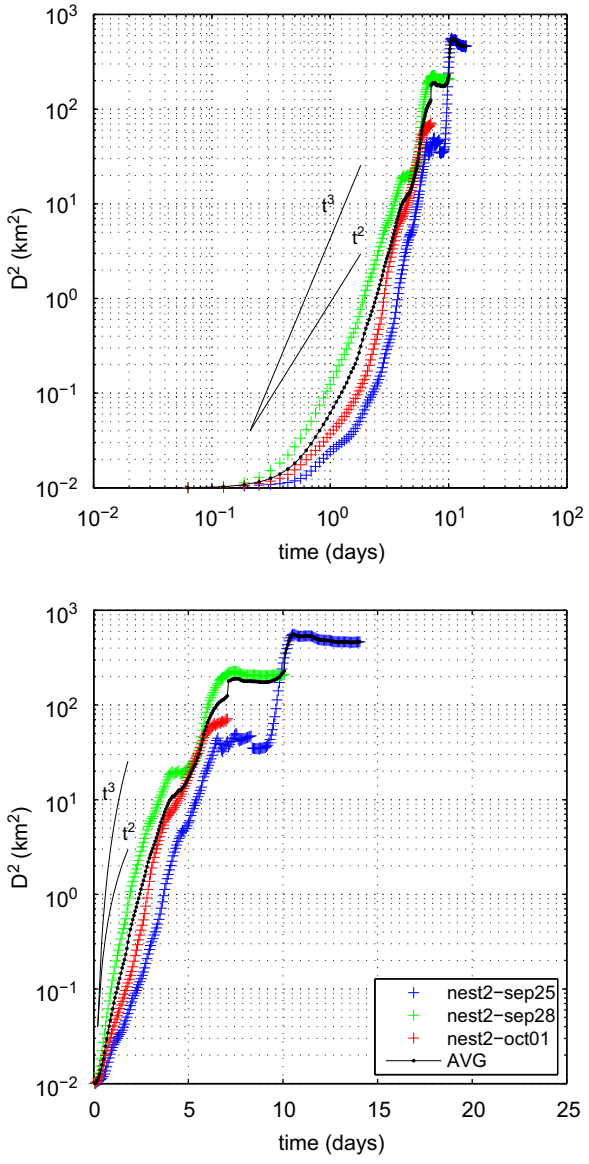

Fig. 17. (Upper panel) log–log, (lower panel) log–linear plots of $D^2(t)$ from NCOM for nest2 from launches targeted at similar initial regions as in the field experiments.

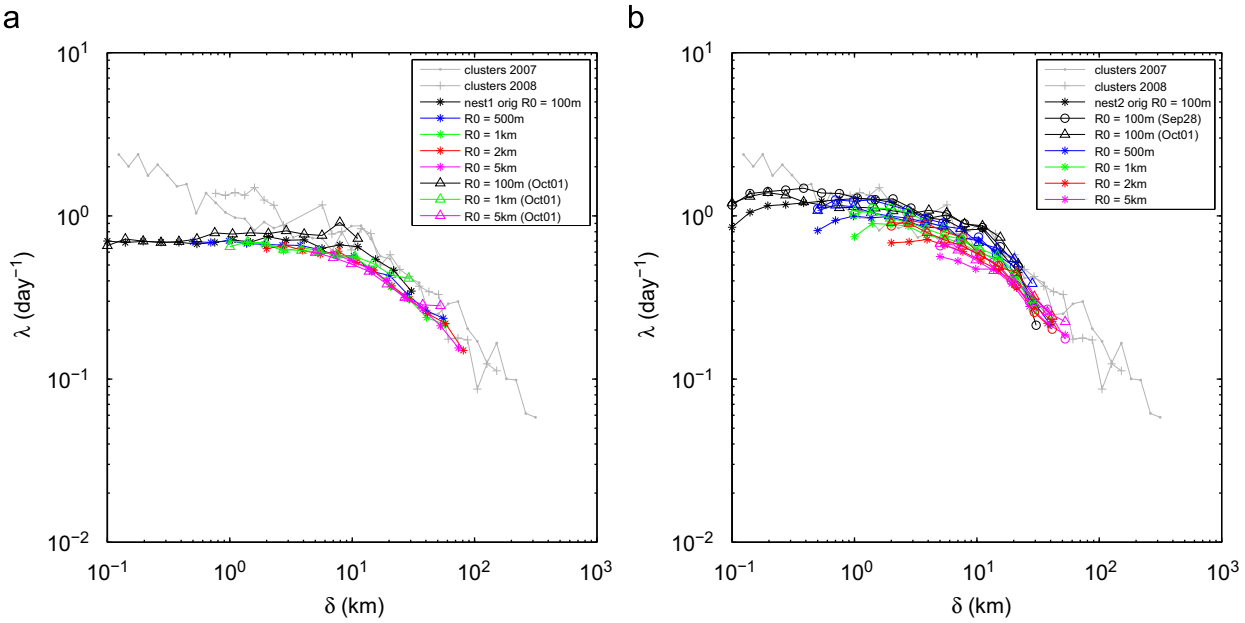

Fig. 18. $\lambda(\delta)$ from the original pairs with r_0=0.1, 1, 2 and 5 km for (a) nest1 and (b) nest2. The FSLE curves $\lambda(\delta)$ from CODE drifters are plotted in the background.

This behaviour might be related to emergence of strong divergence zones in the model surface fields at 0.6 km resolution. Nevertheless, this study is focussed only on the 2D relative dispersion problem, and investigation of any significant 3D effects on relative dispersion will be undertaken in future studies.

In order to shed some light into errors caused by sampling issues, the same computations are carried out by using only the center particles (namely ignoring the satellite particles). We recall that the center particles are 5.4 (3) km apart in nest1 (nest2), so that only chance pairs are available below those scales. The results are shown in Fig. 19a and b for nest1 and nest2, respectively. In both cases, there is a good agreement between the results from synthetic and real drifters. Nevertheless, we know that model results contain errors in that the pair numbers reduce by one to two orders of magnitude for $\delta < 1$ km in chance pairs with respect to original pairs (Fig. 19c and d). As such, original pair computation is more reliable than the one based on chance pairs for these scale separations. The results attained here are consistent with those in Haza et al. (2008) in that the FSLE plateau is less clear, and the limiting value λ_{max} is overestimated when chance pairs instead of original pairs are used. In particular, we see a factor of 2 in λ_{max} when the pair number is reduced from 2000 to 20 in nest1, while it is even more stringent for nest2; a factor of two of overestimation of λ_{max} when the pair number decreases from 3000 (original) to 200 (chance).

The difference between the reference original pair results (red lines) and the chance pair results (blue lines) in Fig. 19a and b is likely to be due to two competing effects: the decrease in number of available pairs when using chance pairs at small δ and the nature of chance pairs, related to possible dynamical biases. In order to distinguish between these two factors, we have performed a further computation shown in Fig. 20, where the number of pairs is gradually decreased by subsampling the original pairs, from 3000 down to only 12. The corresponding results in the λ estimates (Fig. 20a) appear stable at decreasing number of pairs down to 23 pairs, and even for 12 pairs the estimate appears to oscillate around the reference value. In order to compare the results in Figs. 20a and 19a for approximately the same number of pairs, we consider, for instance, the range $\delta \approx 1$ km. The corresponding number of chance pairs shown by the curve behaviour in Fig. 19c is approximately 50. The chance pair result (Fig. 19a) can then be roughly compared to the results for 50 original pairs in Fig. 20a. The original pair results show a clearer plateau and appear closer to the reference value. This indicates that, at a given number of pairs, original pairs provide more reliable results than chance pairs, in agreement with previous results by Haza et al. (2008).

We notice that the real drifter results rely on original pairs in the range $\delta \approx 1$ km, that corresponds to the range of the initial launching distances in the clusters, but the number of original pairs drastically decrease for $\delta < 1$ km and $\delta > 6$ km. Ultimately, the present results call for ocean experiments with significantly higher number of drifters at various scales than ever conducted thus far in order to identify relative dispersion in the sub-mesoscale range.

5. Summary and conclusions

In this paper we investigate the properties of relative dispersion using a set of data from clusters of 3–5 drifters in the Ligurian Sea during two MREA experiments, in 2007 and 2008, respectively. The total data set consists of 45 original pairs with initial distances of less than 1 km and of more than 50 chance pairs in the spatial range between 1 and 200 km. We focus mostly on the initial phase of relative dispersion, when more data are available, and on space scales ranging from less than 1 km to the mesoscale, i.e. 10–20 km. The data are analyzed using two independent metrics, the mean square separation of particle pairs $D^2(t)$, that is a function of time from release, and the FSLE, which is a function of separation scale.

The two metrics show consistent results, indicating an initial phase of dispersion characterized by a clear exponential behaviour with an e-folding time scale T_D between 1/2 and 1 days, and Lyapunov exponent λ in the range 0.7–1.5 days^{-1}. The exponential phase extends for 4–7 days in time and for more than a decade between 1 and 10–20 km in space. The exponential phase is followed by a different regime whose characteristics cannot be quantitatively assessed especially for $D^2(t)$ because of the restricted number of available pairs. Both $D^2(t)$ and FSLE statistics, though, suggest a power law behaviour, in between Richardson and ballistic, consistent with the fact that most drifters are entrained in the NC and in its recirculations, characterized by high horizontal shear.

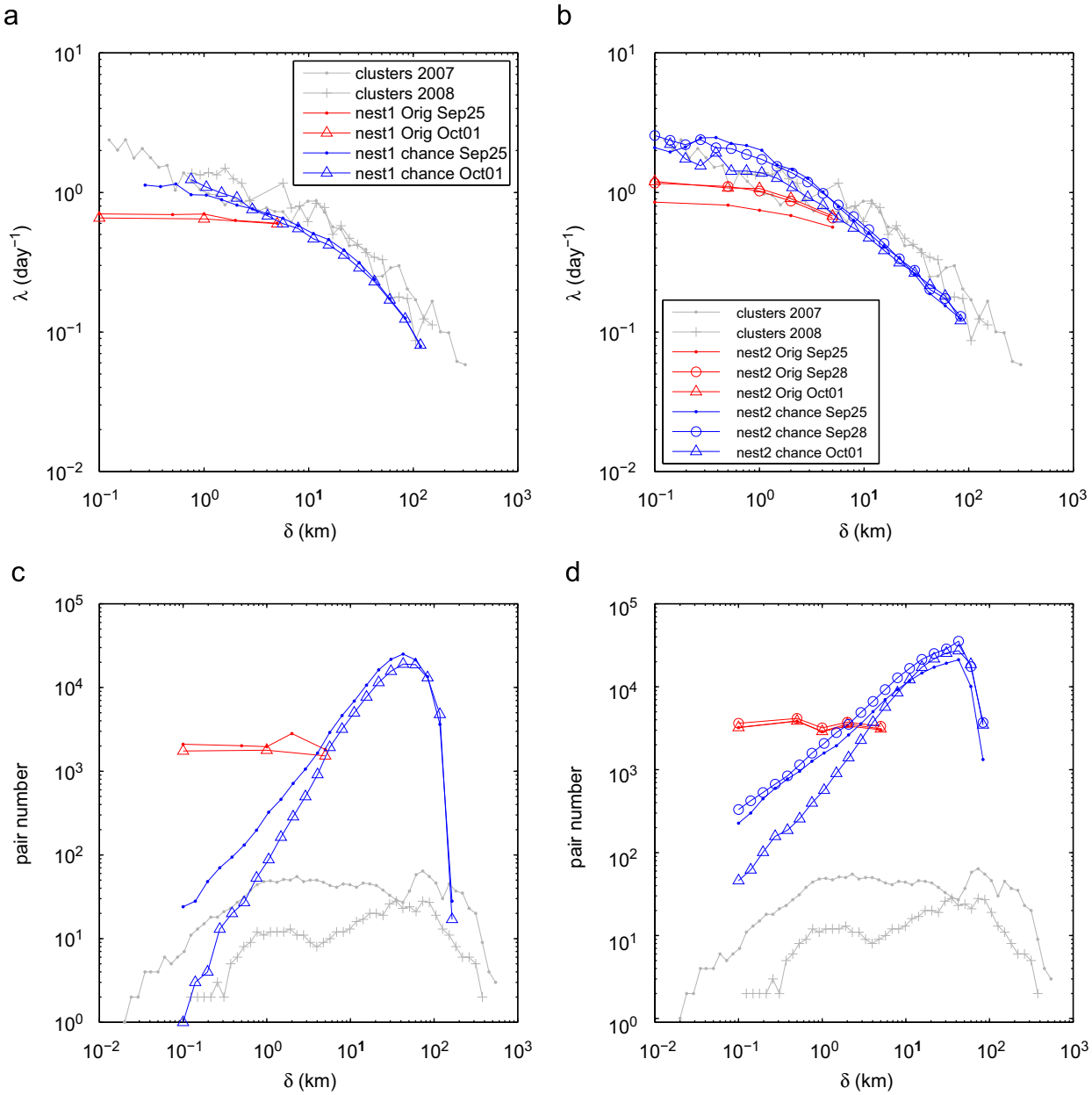

Fig. 19. $\lambda(\delta)$ for (a) nest1 and (b) nest2 domains from chance pairs (blue) and original pairs (red) launched at different dates (dots: September 25; circles: September 28; triangles: October 1, 2008). Results from MREA07 and MREA08 clusters are shown in grey. Number of pairs available for computation in (c) nest1 and (d) nest2 domains. (For interpretation of the references to color in this figure legend, the reader is referred to the web version of this article.)

The results from drifter data have been complemented by an investigation using synthetic drifter data from the NCOM model that has been run in real time during the 2008 experiment at two different resolutions of 1.8 km (nest1) and 0.6 km (nest2), respectively. Results for both resolutions are qualitatively consistent with the drifter results, showing an initial exponential behaviour with corresponding $\lambda \approx 0.6$ days^{-1} for nest1 and 1 days^{-1} for nest2. The increase of λ at increasing resolution (almost a doubling from nest1 to nest2) corresponds to an increase in the Okubo–Weiss parameter that quantifies the hyperbolicity of the velocity field, in agreement with what found in previous works (Poje et al., 2010). Model results have also been used to investigate sampling issues in computing relative dispersion. Reference estimates have been first computed using a data set consisting of a high number of original pairs (2000–3000 pairs available up to $\delta < 1$ km). These results are compared with those obtained from chance pairs released at 5–3 km. In this case, the pair number decreases strongly for small distances δ and the FSLE plateau is less clear with a limiting value that is up to a factor 2 bigger than the reference one. When instead original pairs are subsampled, decreasing their number down to 20–10, the FSLE plateau is more clear, and the estimates of λ appear to oscillate around the reference value.

To our knowledge, this is only the third time that an exponential regime is observed from drifter data. Our results are consistent with those of LaCasce and Ohlmann (2003) and Koszalka et al. (2009) who found an exponential regime in the Gulf of Mexico and in the Nordic Seas, respectively. Also the e-folding time scales T_D and λ are qualitatively similar, given that LaCasce and Ohlmann (2003) finds $T_D \approx 2-3$ days and Koszalka et al. (2009) 0.5 day. Values in the same range have also been found previously in numerical model results (Haza et al., 2008). Markedly different values instead, have been found by Haza et al. (2010) from the analysis of HF radar in the Gulf of La Spezia, characterized by significantly higher λ and smaller T_D. This is likely to be due to the

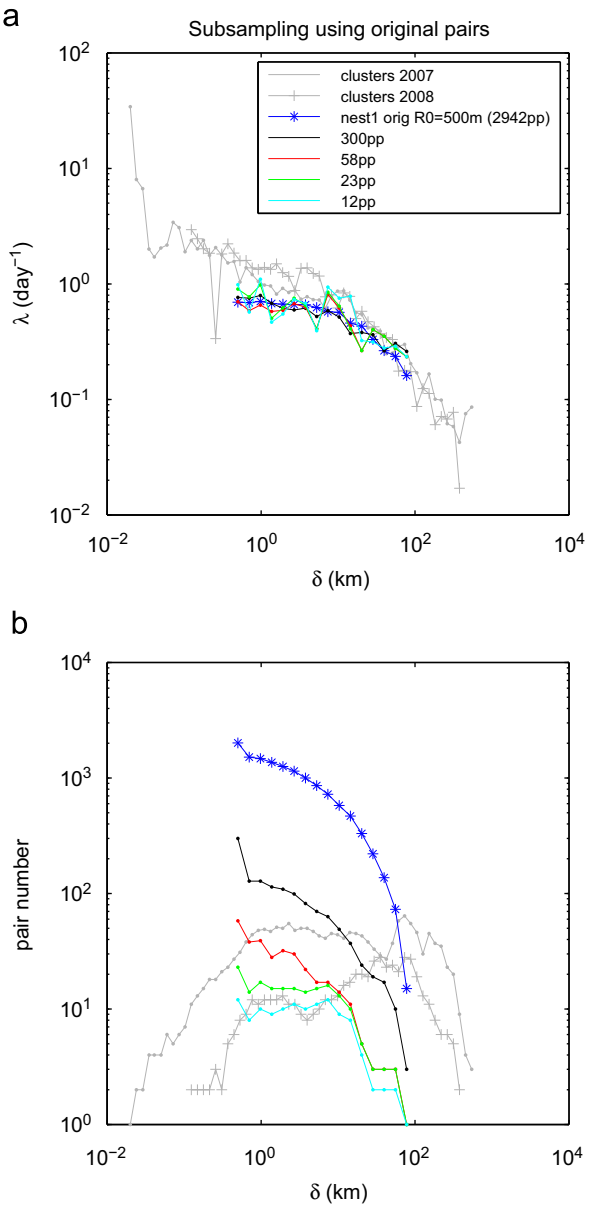

Fig. 20. (a) $\lambda(\delta)$ for nest1 domain from subsampled original pairs. Results from MREA07 and MREA08 clusters are shown in grey. (b) Number of pairs available for computation.

smaller scales of the coastal flows in the Gulf, that has dimension of the order of 10 km. Finally, we point out to the remarkable differences with the results of Lumpkin and Elipot (2010) in the Gulf Stream region, not only in terms of λ values but also in the terms of regimes. Lumpkin and Elipot (2010), in fact, find that the initial phase of relative dispersion is characterized by a power law rather than by an exponential. The reasons for this difference are not clear at the moment and need further investigation. It might be due to the difference in geographical regions, characterized by different dynamical properties (Griffa et al., 2008), or it might be due to unusual (stormy) conditions occurring during the launches.

The initial exponential regime observed here is suggestive of the fact that relative dispersion in the Liguro-Provençal basin is predominantly nonlocal, namely the strain field created by the mesoscale dynamics dictates relative dispersion in the sub-mesoscale range. This is consistent also with the patterns of the trajectories in the clusters and with the velocity field as sampled by the drifters. Semi-permanent mesoscale structures and recirculations with scales of the order of 10–20 km are clearly visible in the velocity field, and most of the drifters appear to be initially captured inside them, moving coherently together and progressively separating until they reach the scale of the recirculations. In addition, an operational ocean model with a mesoscale eddy field representative of the region appears to have attained a reasonable agreement with drifter data in terms of relative dispersion, within the accuracy feasible from the existing observations.

This result has a number of implications. First and foremost, it puts not only the role of sub-mesoscale processes in ocean transport in doubt, but also fundamentally questions their existence in the ocean circulation, naturally leading to the following issues. Are the sub-mesoscale turbulent features pervasive in the upper ocean, or are they episodic in time, and maybe confined only to certain regions? If they are pervasive, how can they be detected using current observational methods, if their effect on transport is quite small in comparison to that by the mesoscale features? If they do not influence ocean transport, in which other ways are they important? Can they coexist with mesoscale features? We believe that all of these questions are open and deserve to their own investigation as resources and technology allow. These questions are posed on the basis of the present study, and several other observational and modeling studies mentioned above. Given the still small number of regions studied, it remains to be seen how broad is the applicability of our conclusions, but certainly it is not clear at the present time that sub-mesoscale processes are prevalent in the upper ocean.

Second, the result that an eddy-resolving model with only approximate representation (both in terms of exact location and speed, and also resolution) of the mesoscale features allows for statistical transport estimation at all scales in this region supports the applicability of Lagrangian transport view on the basis of 2D geometrical features to the ocean circulation, or at least, it does not contradict the perspective brought by this school of thought.

Third, this result paves the way toward a number of practical applications. The potential for neglect of an unknown degree of sub-mesoscale induced stirring and mixing allows a quick estimation of an initial behaviour of pollutants in the upper ocean. In the Liguro-Provençal basin, we can expect that an initial patch will tend to grow in size exponentially with a doubling time of approximately 0.5–1 days, until it reaches a scale of $\approx$20 km, corresponding to the main recirculating structures. Such scales are of the order of the local deformation radius, and are likely to be due to the combination of baroclinic instabilities and topographic constraints. Furthermore, accurate estimation of the pollutant's spreading should be feasible on the basis of eddy-resolving, data-assimilating ocean models (provided that the pollutant acts as a passive particle, or scalar field). This is very relevant for first action planning and mitigation in case of accidents at sea, providing information on an expected initial behaviour of the pollutant.

As a final remark, we notice that a few drifters show a qualitatively different behaviour with respect to the dominant one described above. A few drifter pairs, in fact, are observed to leave the main cyclonic gyre and its recirculations and get stranded in a region in the eastern Ligurian Sea, characterized by shallower depths and lower energy. These pairs tend to be trapped in this area for a period of almost a month, and their behaviour in terms of relative dispersion appears at least qualitatively different, since they tend to separate and then to get closer again, so that after 20 days their average distance is still less than 20 km. At the moment, there are not enough data from the drifters nor from the model (that does not reproduce the dynamics of this area correctly), to investigate this phenomenon in a quantitative way. A possible hypothesis is that the dynamics in this region is different from the rest of the Liguro-Provençal basin, and possibly influenced by

sub-mesoscale processes related to the presence of a number of small scale surface fronts. This could still be suggestive in that different geographical regions, even in the same area, could have different dynamical properties in terms of relative dispersion. Dedicated experiments are planned to further investigate this aspect.

Acknowledgements

This research was supported by Office of Naval Research under Grants N00014-05-1-0094 and N00014-05-1-0095 (Haza, Özgökmen, Griffa), by NRL under Grant N00173-07-2-C901 (Peggion), by the ECOOP (EU) project (Griffa) and by the North Atlantic Treaty Organization (Rixen). Fruitful collaborations with N. Pinardi, G. Gasparini and A. Molcard are acknowledged. We thank all the people who have helped with the drifter deployment and recovery operations. We would also like to thank three anonymous reviewers for their constructive criticism that has helped to improve the manuscript significantly.

References

Artale, V., Boffetta, G., Celani, A., Cencini, M., Vulpiani, A., 1997. Dispersion of passive tracers in closed basins: beyond the diffusion coefficient. Phys. Fluids 9, 3162–3171.

Astraldi, M., Gasparini, G.P., 1992. The seasonal characteristics of the circulation in the North Mediterranean basin and their relationship with the atmospheric climatic conditions. J. Geophys. Res. 97 (C6), 9531–9540.

Astraldi, M., Gasparini, G.P., Sparnocchia, S., 1994. The seasonal and interannual variability in the Ligurian Provencal Basin. Coastal Estuarine Stud. 46, 93–113.

Astraldi, M., Gasparini, G.P., Manzella, G., Hopkins, T.S., 1990. Temporal variability of currents in the Eastern Ligurian Sea. J. Geophys. Res. 95 (C2), 1515–1522.

Aurell, E., Boffetta, G., Crisanti, A., Paladin, G., Vulpiani, A., 1997. Predictability in the large: an extension of the concept of Lyapunov exponent. J. Phys. A 30, 1–26.

Barbanti, R., Iungwirth, R., Poulain, P.-M., 2005. Stima dell'accuratezza del drifter tipo CODE con GPS nella determinazione della posizione geografica. Rel. 32/2005/OGA/20, OGS, Trieste, Italy.

Barth, A., Alvera-Azcratea, A., Rixen, M., Beckers, J.-M., 2005. Two-way nested model of mesoscale circulation features in the Ligurian Sea. Prog. Oceanogr. 68, 171–189.

Bauer, S., Swenson, M.S., Griffa, A., 2002. Eddy mean flow decomposition and eddy diffusivity estimates in the tropical Pacific Ocean: 2. Results. J. Geophys. Res. Oceans 107, 3154. doi:10.1029/2000JC000613.

Bennett, A.F., 1984. Relative dispersion—local and nonlocal dynamics. J. Atmos. Sci. 41 (11), 1881–1886.

Capet, X., McWilliams, J.C., Molemaker, M.J., Shchepetkin, A., 2008. The transition from mesoscale to submesoscale in the California current system: frontal processes. J. Phys. Oceanogr. 38, 44–64.

Coulliette, C., Wiggins, S., 2000. Intergyre transport in a wind-driven, quasigeostrophic double gyre: an application of lobe dynamics. Nonlinear Processses Geophys. 7, 59–85.

Crepon, M., Wald, L., Monget, J.-M., 1982. Low-frequency waves in the Ligurian Sea during December 1977. J. Geophys. Res. 87 (C1), 595–600.

Davis, R.E., 1985. Drifter observation of coastal currents during CODE. The method and descriptive view. J. Geophys. Res. 90, 4741–4755.

d'Ovidio, F., Fernandez, V., Hernandez-Garcia, E., Lopez, C., 2004. Mixing structures in the Mediterranean Sea from finite-size Lyapunov exponents. Geophys. Res. Lett. 31, L17203. doi:10.1029/2004GL020328.

Ehlmaidi, D., Provenzale, A., Babiano, A., 1993. Elementary topology of two-dimensional turbulence from a Lagrangian viewpoint and single particle dispersion. J. Fluid Mech. 257, 533–558.

Emery, W.J., Thomson, R.E., 2004. Data Analysis Methods in Physical Oceanography, second ed. Elsevier, Amsterdam, The Netherlands 638pp.

Fabbroni, N., 2009. Numerical simulations of passive tracers dispersion in the sea. Ph.D. Thesis, University of Bologna, 164 pp.

Griffa, A., Lumpkin, R., Veneziani, M., 2008. Cyclonic and anticyclonic motion in the upper ocean. Geophys. Res. Lett. 35, L01608. doi:10.1029/2007GL032100.

Haller, G., 1997. Distinguished material surfaces and coherent structures in three-dimensional flows. Physica D 149/4, 248–277.

Haller, G., Poje, A., 1998. Finite time transport in aperiodic flows. Physica D 119, 352–380.

Hansen, D.V., Poulain, P.-M., 1996. Processing of WOCE/TOGA drifter data. J. Atmos. Oceanic Technol. 13, 900–909.

Haza, A.C., Griffa, A., Martin, P., Molcard, A., Özgökmen, T.M., Poje, A.C., Barbanti, R., Book, J.W., Poulain, P.M., Rixen, M., Zanasca, P., 2007. Model-based directed drifter launches in the Adriatic Sea: results from the DART experiment. Geophys. Res. Lett. 34. doi:10.1029/2007GL029634.

Haza, A.C., Özgökmen, T.M., Griffa, A., Molcard, A., Poulain, P., Peggion, G., 2010. Transport properties in small scale coastal flows: relative dispersion from VHF radar measurements in the Gulf of La Spezia. Ocean Dyn. 60, 861–882.

Haza, A.C., Poje, A., Özgökmen, T.M., Martin, P., 2008. Relative dispersion from a high-resolution coastal model of the Adriatic Sea. Ocean Modelling 22, 48–65.

Herbaut, C., Mortier, L., Crpon, M., 1997. A sensitivity study of the general circulation of the western Mediterranean. Part II: the response to atmospheric forcing. J. Phys. Oceanogr. 27, 2126–2145.

Klein, P., Hua, B.L., Lapeyre, G., Capet, X., Le Gentil, S., Sasaki, et H., 2008. Upper ocean turbulence from high 3D resolution simulations. J. Phys. Oceanogr. 38, 1748–1763.

Koszalka, I., LaCasce, J.H., Orvik, K.A., 2009. Relative dispersion statistics in the Nordic Seas. J. Mar. Res. 67, 411–433.

Kraichnan, R.H., 1967. Inertial ranges in two-dimensional turbulence. Phys. Fluids 10, 1417–1423.

LaCasce, J., Bower, A., 2000. Relative dispersion in the subsurface north atlantic. J. Mar. Res. 58, 863–894.

LaCasce, J., Ohlmann, C., 2003. Relative dispersion at the surface of the Gulf of Mexico. J. Mar. Res. 61 (3), 285–312.

Lacorata, G., Aurell, E., Vulpiani, A., 2001. Drifter dispersion in the adriatic sea: Lagrangian data and chaotic model. Ann. Geophys. 19, 121–129.

Lacorata, G., Aurell, E., Legras, B., Vulpiani, A., 2004. Evidence for a spectrum from the EOLE Lagrangian balloons in the low stratosphere. J. Atmos. Sci. 61, 2936–2942.

Lumpkin, R., Elipot, S. 2010. Surface drifter pair spreading in the North Atlantic. Journal of Geophysical Research 115, C12017, doi:10.1029/2010JC006338.

Lumpkin, R., Pazos, M., 2007. Measuring surface currents with surface velocity program drifters: the instrument, its data, and some recent results. In: Griffa, A., Kirwan, A.D., Mariano, A., Zgkmen, T., Rossby, T. (Eds.), Chapter 2 of "Lagrangian Analysis and Prediction of Coastal and Ocean Dynamics". Cambridge University Press.

Marullo, S., Salusti, E., Viola, A., 1985. Observations of a small scale baroclinic eddy in the Ligurian Sea. Deep-Sea Res. 32, 215–222.

Martin, P.J., 2000. Description of the navy coastal ocean model version 1.0. Naval Research Laboratory Report RL/FR/7322-00-9962, 42 pp.

Miller, P., Pratt, L., Helfrich, K., Jones, C., 2002. Chaotic transport of mass and potential vorticity for an island recirculation. J. Phys. Oceanogr. 32, 80–102.

Millot, C., 1991. Mesoscale and seasonal variabilities of the circulation in the western Mediterranean. Dyn. Atmos. Oceans 15 (3–5), 179–214.

Molcard, A., Poje, A., Özgökmen, T., 2006. Directed drifter launch strategies for lagrangian data assimilation using hyperbolic trajectories. Ocean Modelling 12, 268–289.

Mounier, F., Echevin, V., Mortier, L., Crpon, M., 2005. Analysis of the mesocale circulation in the occidental Mediterranean Sea during winter 1999–2000 given by a regional circulation model. Prog. Oceanogr. 66, 251–269.

Okubo, A., 1970. Horizontal dispersion of floatable particles in vicinity of velocity singularities such as convergences. Deep-Sea Res. 17 (3), 445–454.

Okubo, A., 1971. Oceanic diffusion diagrams. Deep-Sea Res. 18, 789–802.

Olascoaga, M., Rypina, I.I., Brown, M.G., Beron-Vera, F.J., Kocak, H., Brand, L.E., Halliwell, G.R., Shay, L.K., 2006. Persistent transport barrier on the West Florida Shelf. Geophys. Res. Lett. 33, 22603. doi:10.1029/2006GL027800.

Ollitrault, M., Gabillet, C., de Verdiere, A.C., 2005. Open ocean regimes relative dispersion. J. Fluid Mech. 533, 381–407.

Ovchinnikov, I.M., 1966. Circulation in the surface and intermediate layers of the Mediterranean. Oceanology 6, 48–59.

Ottino, J., 1989. The Kinematics of Mixing: Stretching, Chaos and Transport. Cambridge University Press.

Poje, A., Haller, G., 1999. Geometry of cross-stream mixing in a double-gyre ocean model. J. Phys. Oceanogr. 29, 1649–1665.

Poje, A., Haza, A., Özgökmen, T., Magaldi, M., Garraffo, Z., 2010. Resolution dependent relative dispersion statistics in a hierarchy of ocean models. Ocean Modelling 31, 36–50.

Poulain, P.-M., 1999. Drifter observations of surface circulation in the Adriatic Sea between December 1994 and March 1996. J. Mar. Syst. 20, 231–253.

Poulain, P.-M., 2001. Adriatic Sea surface circulation as derived from drifter data between 1990 and 1999. J. Mar. Syst. 29, 3–32.

Poulain, P.-M, Gerin, R., Rixen, M., Zanasca, P., Teixeira, J., Griffa, A., Molcard, A., De Marte, M., Pinardi, N. Surface circulation in the Liguro-Provencal basin as measured by satellite-tracked drifters (2007–2009). Ocean Dyn., submitted for publication. Available from: 〈http://www.rsmas.miami.edu/personal/tamay/misc/PMPetal2010.pdf〉.

Rixen, M., Coelho, E., 2007. Operational surface drift prediction using linear and non-linear hyper-ensemble statistics on atmospheric and ocean models. J. Mar. Syst. 65, 105–121.

Rixen, M., Coelho, E., Signell, R., 2008. Surface drift prediction in the Adriatic Sea using hyper-ensemble statistics on atmospheric, ocean and wave models: uncertainties and probability distribution areas. J. Mar. Syst. 69, 86–98.

Rivera, M., Ecke, R., 2005. Pair dispersion and doubling time statistics in two-dimensional turbulence. Phys. Rev. Lett. 95 (19), 194503.

Salmon, R., 1980. Baroclinic instability and geostrophic turbulence. Astrophys. Fluid Dyn. 10, 25–52.

Sammari, C., Millot, C., Prieur, L., 1995. Aspects of the seasonal and mesoscale variabilities of the Northern current in the western Mediterranean Sea inferred from the PROLIG-2 and PROS-6 experiments. Deep-Sea Res. I 42, 893–917.

Sawford, B., 2001. Turbulent relative dispersion. Ann. Rev. Fluid Mech. 33, 289–317.

Shadden, S., Lekien, F., Paduan, J.D., Chavez, F.C., Marsden, J.E., 2008. The correlation between surface drifters and coherent structures based on high-frequency data in Monterey Bay. Deep-Sea Res. II 56, 161–172.

Toner, M., Poje, A.C., 2004. Lagrangian velocity statistics of directed launch strategies in a Gulf of Mexico model. Nonlinear Processses Geophys. 11, 35–46.

Vandenbulcke, L., Beckers, J., Lenartz, F., Barth, A., Poulain, P., Aidonidis, M., Meyrat, J., Ardhuin, F., Tonani, M., Fratianni, C., Torrisi, L., Pallela, D., Chiggiato, J., Tudor, M., Book, J.W., Martin, P., Peggion, G., Rixen, M., 2009. Super-ensemble techniques: application to surface drift prediction during the DART06 and MREA07 campaigns. Prog. Oceanogr. 82, 149–167.

Vignudelli, S., Cipollini, P., Reseghetti, F., Fusco, G., Gasparini, G.P., Manzella, G.M.R., 2003. Comparison between XBT data and TOPEX/Poseidon satellite altimetry in the Ligurian–Tyrrhenian area. Ann. Geophys. 21, 123–135.

Weiss, J., 1991. The dynamics of enstrophy transfer in 2-Dimensional hydrodynamics. Physica D 48 (2–3), 273–294.

Wiggins, S., 2005. The dynamical systems approach to Lagrangian transport in oceanic flows. Ann. Rev. Fluid Mech. 37, 295–328.